3 Peroxy radical self reactions studied by photoionization mass spectrometry

3.1 Introduction

The work in Chapter 2 was one of the first studies to look at the products from a peroxy radical (RO_2) self reaction on the time scale of the reaction. The downside of that work was that it was only able to follow one product channel. The work described here set out to better characterize the products by monitoring all of the stable product channels on the timescale of the reaction.

The specifics of the $C_2H_5O_2$ chemistry introduced in Chapter 2 can be generalized to a wide range of RO_2 whose atmospheric importance was discussed in Chapter 1. The RO_2 self reaction chemistry generally follows the scheme below.

$$RO_2 + RO_2 \longrightarrow ROH + R'CHO + O_2 \quad (3.1)$$

$$\longrightarrow RO + RO + O_2 \quad (3.2)$$

$$\longrightarrow ROOR + O_2 \quad (3.3)$$

$$RO + O_2 \longrightarrow HO_2 + R'CHO \quad (3.4)$$

$$RO_2 + HO_2 \longrightarrow ROOH + O_2 \quad (3.5)$$

In most cases the RO_2 of interest is generated in the laboratory by reaction of the appropriate alkyl radical (R) with oxygen so the following formation reactions are also important.

$$R + O_2 \xrightarrow{M} RO_2 \quad (3.6)$$

$$R + O_2 \longrightarrow R''CH{=}CH_2 + HO_2 \quad (3.7)$$

There are also competing reactions which need to be accounted for, and they make up part of the general scheme.

$$RO_2 + RO \longrightarrow \text{Products} \qquad (3.8)$$

$$HO_2 + HO_2 \longrightarrow H_2O_2 + O_2 \qquad (3.9)$$

The key physical parameter of interest for this work was the radical channel branching fraction of the RO_2 self reaction (reaction (3.2)) defined as,

$$\alpha = \frac{k_{1.2}}{k_{1.1} + k_{1.2} + k_{1.3}} \qquad \text{i}$$

During this work methyl (CH_3), ethyl (C_2H_5), and propyl (C_3H_7) R groups were investigated. Previous work on the CH_3O_2 self reaction was reviewed by Tyndall et al.[1], work on the $C_2H_5O_2$ self reaction was discussed in Chapter 2, and there have been only two product studies on the i-$C_3H_7O_2$ self reaction.[2,3] Of this previous work only the experiments described in Chapter 2 and high temperature (T > 373 K) work by Lightfoot et al.[4] monitored the nascent products on the timescale of the reaction. All of the other studies analyzed the stable end products by FTIR, GC, and GC/MS seconds to minutes after the reaction. The work in Chapter 2 measured a value for α a factor of two lower than the end product studies found for the $C_2H_5O_2$ self reaction by measuring the secondary HO_2 formed from reactions (3.2) and (3.7) using near-infrared kinetics spectroscopy. This work set out to determine whether detection of all the stable products on the time scale of the reaction using a photoionization mass spectrometer technique could determine the cause of the discrepancy between previous end product studies and the work in Chapter 2.

3.2 Experimental

A flash photolysis flow cell coupled to a photoionization mass spectrometer was used to study the product branching ratio of reactions (3.1) – (3.3). The RO_2 chemistry was initiated by laser photolysis and then reacted throughout the laminar flow cell. As the plug flow moved down the flow cell it was sampled from a pinhole at the midpoint of the cell. The sampled gas expanded into the ionization region where it was ionized by the synchrotron radiation. Ion optics then focused a beam into the mass spectrometer where a sector magnet separated the masses for simultaneous detection with a micro-channel plate detector. The product masses were identified by their time traces as well as characteristic ionization energies. The branching fraction was determined by measuring the ratio of the product masses as well as by conversion to absolute concentrations combined with kinetics modeling.

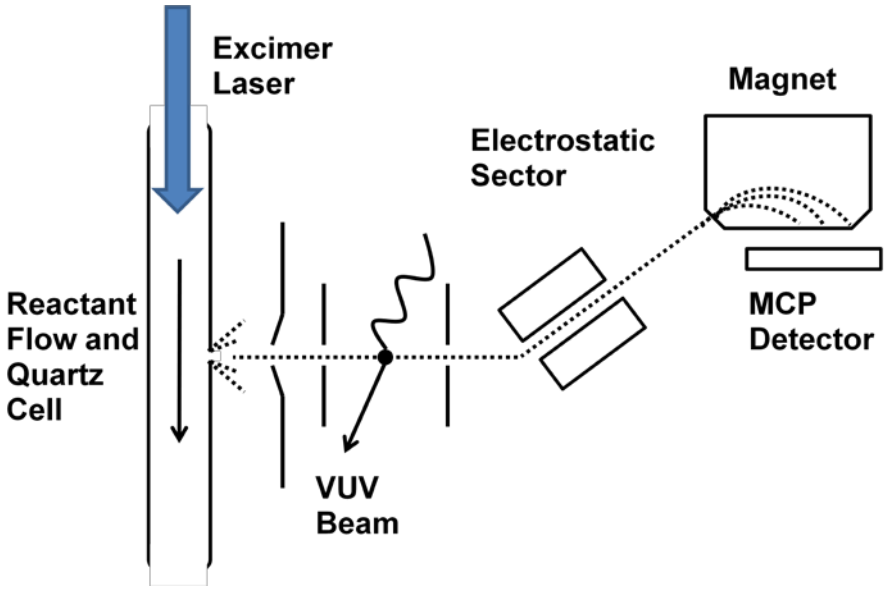

Figure 3-1. Schematic of experimental system

A schematic of the experiment is shown in **Figure 3-1**, and the full apparatus has been described previously.[5] The flow tube was 60 cm long with a 600 μm pinhole 35 cm from the entrance. Mass flow controllers delivered the precursor gases to the cell where

the total pressure was controlled by an automated feedback throttle valve leading to a vacuum pump. Typical flow velocities were ~400 cm s^{-1} allowing for a fresh fill of precursor gas for every photolysis pulse.

Ionizing synchrotron undulator radiation came from the Advanced Light Source (ALS) at Lawrence Berkeley National Lab, and was dispersed using a 3 m monochromator on the Chemical Dynamics Beamline. A 30 Torr Ar gas filter suppressed higher undulator harmonics. The radiation energy could be scanned during a data set with energy resolution of 40 – 80 meV corresponding to a monochromator slit width of 0.6 – 1 mm. Energy calibration was done using Ar absorbance using the Ar gas filter as an absorption cell, O_2 autionization resonances, and Xe atomic resonances.

The quasi-continuous synchrotron light passed through the ionization region of a miniature double-focusing magnetic-sector mass spectrometer of the Mattauch-Herzog geometry. Ions were dispersed according to the square root of their mass in a 0.94 T magnetic field. A time and position sensitive multi-channel plate detector with a delay line anode recorded the position and time relative to the photolysis pulse for each ion. The time resolution of the detector and electronics was ~ 20 ns and the overall time resolution of the experiment including sampling from the pinhole was ~ 50 μs. The mass resolution varied, but for the usable data in Runs 1 and 2 it was 0.70 amu FWHM.

The $C_2H_5O_2$ system was investigated during three separate runs, and the CH_3O_2 and $C_3H_7O_2$ systems were each tried for one run. The precursor chemistry, photolysis laser, and number of averages for each data set are described for each of the RO_2 below. All measurements were performed at room temperature. Each data set also had a signal calibration run where a mixture of known concentrations of ethene, propene, and cis-2-

butene was flown through the cell so that a calibration factor relating counts to concentration could be determined.

3.2.1 $C_2H_5O_2$ system

3.2.1.1 Run 1 (02/27/08–02/28/08)

During Run 1 two types of precursor chemistry were used; Oxalyl chloride (OxCl)/ethane/oxygen mixtures, and diethyl ketone (DEK)/oxygen mixtures. Ethyl radicals were either generated by reaction of Cl, from photolysis of OxCl,with ethane,[6]

$$(\mathrm{ClCO})_2 \xrightarrow{h\nu\ (248)} \mathrm{Cl} + \mathrm{CO} + \mathrm{ClCO}^* \tag{3.10}$$

$$\mathrm{ClCO}^* \longrightarrow \mathrm{Cl} + \mathrm{CO} \tag{3.11}$$

$$\mathrm{Cl} + \mathrm{C_2H_6} \longrightarrow \mathrm{HCl} + \mathrm{C_2H_5} \tag{3.12}$$

or by photolysis of DEK.[7-9]

$$(\mathrm{C_2H_5})_2\mathrm{CO} \xrightarrow{h\nu\ (248\ \mathrm{nm})} \mathrm{C_2H_5} + \mathrm{C_2H_5CO}^* \longrightarrow 2\mathrm{C_2H_5} + \mathrm{CO} \tag{3.13}$$

In both generation methods the ethyl radicals went on to react with oxygen to form $C_2H_5O_2$ by reaction (3.6).

The concentrations for the OxCl chemistry in molecules cm^{-3} were, O_2 = 1.3 x 10^{16}, OxCl = 5.0 x 10^{14} (vapor pressure of 30 Torr at 2 °C), and C_2H_6 = 1.3 x 10^{15}. The helium (He) bath gas was varied to reach total pressures over the range 1 – 6 Torr. Four data sets were taken for the branching ratio measurements with the synchrotron energy set to 10.7 eV. The flash photolysis was done using a KrF excimer laser at 248 nm. 7500 photolysis pulses were averaged at a repetition rate of 4 Hz. One photoionization efficiency (PIE) scan was also performed over the synchrotron energy range 8.6 – 10.7

eV with a 0.025 eV step size and 250 photolysis pulses per step. It was performed at a total pressure of 4 Torr with the same concentrations as the single energy runs.

The DEK chemistry used the same O_2 and He bath concentrations as well as 1.6 x 10^{13} DEK (vapor pressure of 10 Torr at 17.2 °C).[10] Pressure was varied over the range 1 – 6 Torr, and the synchrotron radiation and flash photolysis laser were set to 10.7 eV and 248 nm respectively. Three data sets were taken, and 5000 – 7000 photolysis pulses were averaged for each data set. No PIE scan was done with the DEK chemistry.

3.2.1.2 Run 2 (03/08/08)

Only OxCl chemistry was used for the four branching ratio data sets in this run. Data was taken at total pressures of 4 and 6 Torr. OxCl concentrations were one order of magnitude lower than Run 1, i.e., 5.0 x 10^{13} molecules cm^{-3}. O_2 was the same except for one run at 6 Torr where O_2 was increased to 4.9 x 10^{16} to look for any competition between reactions (3.4) and (3.8). The synchrotron radiation was set at 10.7 eV and three out of four runs were done with flash photolysis at 248 nm. One data set was also done at 193 nm to ensure that there were no complications from reaction of $ClCO^*$ in the 248 nm photolysis. At 193 nm there is no evidence for a stable intermediate, and the net yield of 2Cl + 2CO is reached immediately.[11] The two 6 Torr data sets averaged 3750 photolysis pulses, the 4 Torr/248 nm data set averaged 7500 photolysis pulses, and the 4 Torr/193nm data set averaged 2000 photolysis pulses. An additional data set was taken at a synchrotron radiation of 11.1 eV and 193 nm photolysis where it was possible to observe the photoionization of OxCl. The depletion of the OxCl signal after photolysis was observed to check the alignment of the excimer laser, and insure the expected absorption occurred.

3.2.1.3 Run 3 (12/04/08–12/07/08, poor mass resolution)

During this run the effect of total radical concentration and O_2 were explored. High and low concentrations of each were explored at total pressures of both 4 and 6 Torr. Data on 12/04 was mistakenly taken at one order of magnitude lower O_2 concentration than expected due to the incorrect assignment of mass flow controller in the data acquisition program. The data at 6 Torr of total pressure were taken again at the correct O_2 concentrations. Further experimental problems during this run led to inadequate mass resolution for the products of interest, making reliable branching ratio measurements difficult.

3.2.2 CH_3O_2 system

Acetone/O_2 precursory chemistry was used for the generation of CH_3O_2 radicals. The much slower reaction of chlorine radicals with methane prevents the use of $OxCl/CH_4/O_2$ precursor chemistry for this system. Similar to the DEK chemistry photolysis of acetone is the radical source. At 193 nm the photodissociation is almost exclusively through one product channel.[12]

$$CH_3COCH_3 \xrightarrow{hv,193\ nm} 2CH_3 + CO \quad (>95\%) \tag{3.14}$$

Single photoionization energy data sets using 10.9 eV light were taken at 1 and 4 Torr total pressure. Acetone and O_2 were fixed at 3.8 x 10^{13} and 5 x 10^{16} molecules cm^{-3}, respectively. Acetone was brought into the cell by flowing He through a bubbler filled with acetone held at -31 °C and total pressure 750 Torr. 6000 shots were averaged for each data set. One PIE data set was also taken at 4 Torr total pressure over the range 10 – 11.5 eV. 400 shots per step were taken at a step size of 25 meV. An ArF excimer laser was the source of the 193 nm photolysis pulse, and operated at 4 Hz.

3.2.3 $C_3H_7O_2$ system

For studying the propyl peroxy self reaction both OxCl/C_3H_8/O_2 and Dipropyl ketone (DPK)/O_2 precursor chemistries were used. The OxCl chemistry was not as straightforward in this case because two different H abstraction pathways were in competition leading to two different propyl peroxy radicals. There was a 50/50 split between the primary and secondary propyl radical production,[13] and this led to a variety of products in the self and cross reactions of these two peroxy radicals.

$$Cl + C_3H_8 \longrightarrow CH_2CH_2CH_3 + HCl \ (\sim 50\%) \quad (3.15)$$

$$\longrightarrow CH_3CHCH_3 + HCl \ (\sim 50\%) \quad (3.16)$$

Photolysis of DPK also produced propyl radicals but the yield of reaction (3.17) was not known and other product channels existed.[14]

$$C_3H_7COC_3H_7 \xrightarrow{h\nu, 193\ nm} 2C_3H_7 + CO \quad (3.17)$$

The concentrations for the OxCl chemistry in molecules cm^{-3} were, O_2 = 1.3 x 10^{16}, OxCl = 5.0 x 10^{14}, and C_3H_8 = 1.3 x 10^{15}. A He bath gas brought the total pressure to 1, 4, and 6 Torr. The three single photoionization energy data sets were done at 10.6 eV. The photolysis laser was a KrF excimer at 248 nm operating at 4 Hz, and 2000 – 2500 shots were averaged for each data set. A PIE scan over the range 8.6 – 10.3 eV was also performed at 4 Torr total pressure. The energy resolution was 25 meV and 200 shots were taken at each step.

The DPK chemistry used precursor concentrations of DPK = 1.25 x 10^{13} (V.P. 0.7 Torr at 19 °C)[10] and O_2 = 2.6 x 10^{16} molecules cm^{-3}. A He bath brought the total pressure to 1 or 4 Torr. The three single photoionization data sets were done at 10.6 eV. The

photolysis laser was the ArF excimer at 193 nm and 4 Hz repetition. 5000 shots were averaged for each single energy data set. A PIE scan was done over the range 9.2 – 10.65 eV at a total pressure of 4 Torr. 400 shots per step at a step size of 25 meV were taken for the PIE.

3.3 Results and analysis

This work attempted to measure α for three RO_2 self reactions. A successful measurement was made for $C_2H_5O_2$, and preliminary work was completed for CH_3O_2 and $C_3H_7O_2$. The α value was determined by photoionization mass spectrometry of the time resolved stable end products of the reaction, e.g., acetaldehyde (CH_3CHO), ethanol (C_2H_5OH), and ethyl hydroperoxide (C_2H_5OOH) for the case of the $C_2H_5O_2$ self reaction. Ratios of these products provided a measure of α, as did kinetics fitting to the absolute concentration time profiles. PIE curves were used to help identify products. In addition the first PIE curves of the three ROOH were also measured.

Using equations (ii) and (iii) it was possible to determine α from the ratio of R'CHO and ROH. This relied on assuming the steady state approximation for the concentration of RO in the RO_2 self reaction scheme (3.1) – (3.8), and neglecting reaction (3.3). The observations of ROOR appeared to be from secondary sources in this data so neglecting (3.3) was justified.

$$\alpha = \frac{R-1}{R+1} \qquad \text{ii}$$

$$R = \frac{[\mathrm{R'CHO}]}{[\mathrm{ROH}]} \qquad \text{iii}$$

It was also necessary to know the photoionization cross section of each species to convert the raw value of *R* from the ratio of counts to the ratio of concentrations. The cross sections used were: HCHO = 6.78 Mb and CH_3OH = 1.85 Mb at 10.9 eV,[15,16] CH_3CHO = 7.97 and C_2H_5OH = 3.90 Mb at 10.7 eV,[15,17] C_2H_5CHO = 9.93 Mb and 1-C_3H_7OH = 4.80 Mb at 10.6 eV,[15,18] and CH_3COCH_3 = 11.10 Mb and 2-C_3H_7OH = 0.63 Mb at 10.6 eV.[15] A correction for detection efficiency based on the square root of the mass was also applied when species with large mass differences were compared.[19]

The kinetics fitting method to determine α requires converting counts to the absolute concentrations in order to fit the kinetics of the observed time traces. Calibration data sets for each run were used to determine a calibration factor that converted counts to concentration with the following equation,

$$[\text{Concentration}] = \frac{S}{\sigma * n_{ph} * \Delta t_{bin} * C * \sqrt{m_i}}$$

where *S* is the signal in counts amu$^{0.5}$ timebin^{-1} experiment^{-1} cm^{-1}, σ is the photoionization cross section in MegaBarns (cm^2 molecules^{-1}), n_{ph} is the number of photons in photons s^{-1}, Δt_{bin} is the width of an acquisition time bin in s, *C* is the number of coadded shots, and m_i is the mass in amu of the species. This factor was then scaled for each data set and each species being detected using the appropriate cross section.

Other product ratios were also of interest.

$$R_{A/EH} = \frac{[\text{R'CHO}]}{[\text{ROOH}]}$$

$$R_{E/EH} = \frac{[\text{ROH}]}{[\text{ROOH}]}$$

Without having an independent source for the cross sections of the ROOH it was not possible to make quantitative measurements with these ratios, but they provided insight into the overall reaction mechanism and any deviations from expected behavior.

Single ionization energy runs provided 3D data blocks with the number of counts recorded against axes m/z and time. The data were then examined in a variety of ways. One way was to integrate counts over one m/z unit to look at the time profile of a single mass as is shown in **Figure 3-2**. In each panel one mass has been isolated. A background signal was recorded prior to the self reaction chemistry that was initiated by the excimer laser at 20 ms. The reaction proceeds for ~ 80 ms until the pump out of the reaction flow cell starts to influence the concentration profiles at ~ 100 ms. The remaining trace from 100 – 150 ms follows the pump out of the flow cell. An alternative view of this data, shown in **Figure 3-4**, involved integrating the counts over the time period of the reaction (20 – 100 ms) to look at the full mass spectrum. Both of these views combined with looking at 3D plots allowed careful examination of the data.

PIE data was collected as a 4D data block with the additional axis of photon energy. Three different 3D blocks could be extracted from this data for analysis similar to what was just described for the 3D block at a single photoionization energy. The most common extraction was a 3D block with axes of photon energy and m/z, where the counts have already been integrated along the time axis throughout the 20–100 ms reaction period. This data was then further reduced to look at the mass spectrum or the PIE curve of single masses as shown in **Figure 3-3**.

3.3.1 $C_2H_5O_2$ self reaction

Three different runs were performed on the $C_2H_5O_2$ self reaction. A successful measurement of α was made based off of the results from Runs 1A and 2.

3.3.1.1 Run 1A (OxCl chemistry)

The large number of shots averaged and large radical concentrations led to good signal-to-noise for the OxCl chemistry. No pressure dependence was observed from 1 – 6 Torr in the reaction products. Some higher molecular weight and unknown masses were observed in addition to the expected products. The value for α was successfully determined by both kinetics fitting and *R*.

3.3.1.1.a Observed Products

Figure 3-2 shows the time traces of four stable products from the $C_2H_5O_2$ chemistry including simultaneous kinetic fits using the FACSIMILE program.[20] The products CH_3CHO, C_2H_5OH, and C_2H_5OOH were all observed as expected, and all displayed similar time dependences. Ethene (C_2H_4) from reaction (3.7) was also observed. Its time dependence resembled a step function as it was not produced or consumed after its initial production. Not shown in the figure, C_2H_5 was identified as coming from dissociative ionization of $C_2H_5O_2$ because of its reactant time profile. One feature to note is that the pump out of the flow cell was incomplete for both C_2H_5OH and C_2H_5OOH over the same time scale that it completed for the other two products. The data shown is from the 6 Torr total pressure run, but similar results were observed at 1, 2.5, and 4 Torr as well.

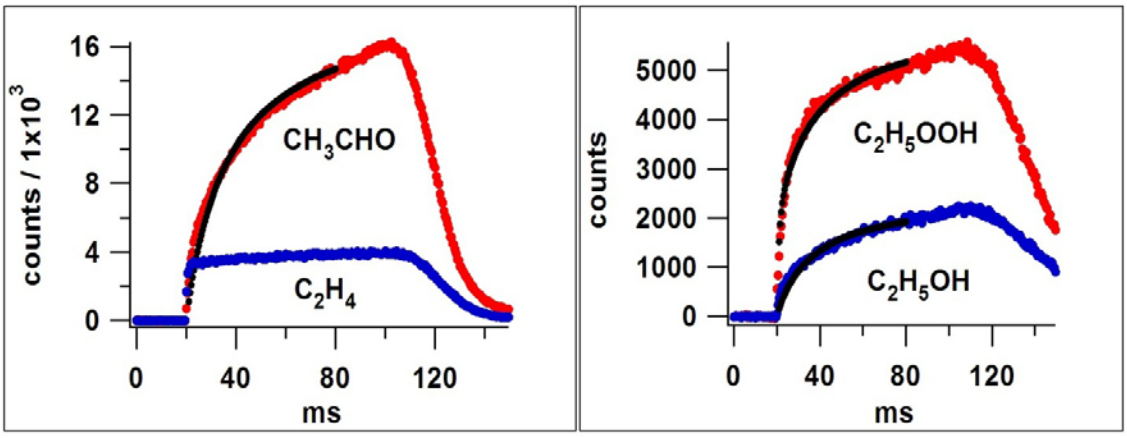

Figure 3-2. Four stable products of the $C_2H_5O_2$ self reaction from OxCl initiation chemistry. The excimer fired at 20 ms and pump out starts ~ 100 ms. The pump out of the ethanol and ethyl hydroperoxide products does not complete on the same time scale as the other two products.

Species assignments were confirmed by looking at the PIE curves and comparing them with the literature. Panel B in **Figure 3-3** shows the comparison between this work and papers by Cool et al. for CH_3CHO and C_2H_4.[15,17] This work did not measure an absolute cross section, but was scaled to the cross sections given in the Cool et al. paper at 10.7 eV for comparison purposes. Good agreements between the curves allowed for definitive identifications. In panel C the agreement between the C_2H_5OH traces was not as good. The qualitative shapes were similar, but the appearance energies were different. The mass resolution in this region was not as good for the PIE data set as shown in Panel A around m/z 46 (C_2H_5OH). It was clear that other masses were likely present as contaminants, but the single energy data sets used for the kinetics analysis, shown in **Figure 3-4**, had much better mass resolution so the qualitative agreement for the ethanol PIE was considered sufficient for identification. No previous PIE for C_2H_5OOH was found in the literature, but the data shown in Panel D had an appearance energy of ~ 9.6 eV in agreement with a first ionization energy of 9.65 eV determined by Li et al. with photoelectron spectroscopy.[21] The cross section values for C_2H_5OOH were determined by

scaling to a value measured at 10.7 eV during Run 2, and will be discussed later during the results from Run 2.

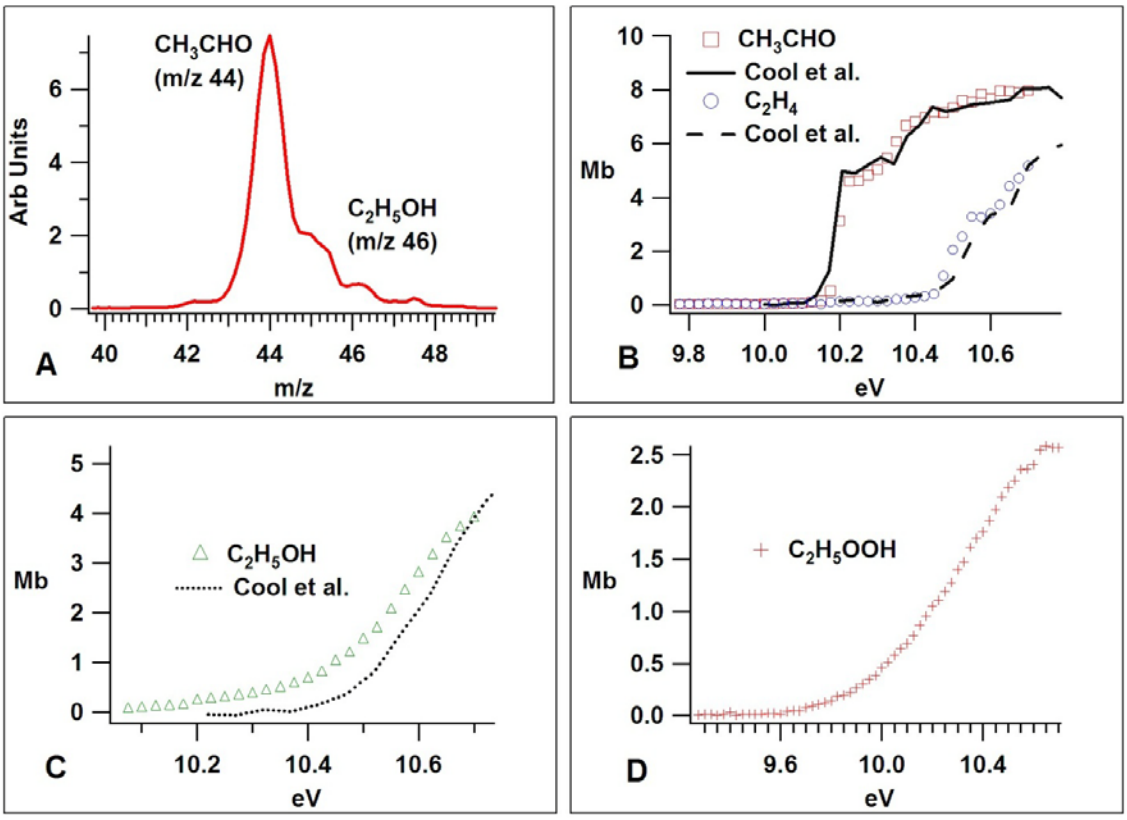

Figure 3-3. (A) 1-D mass spectrum from the PIE data set; the mass resolution was not good in the 4X region. (B) PIE of acetaldehyde and ethene both agreed well with literature. (C) Mass contamination appears to have caused a discrepancy in the ethanol PIE. (D) PIE of ethyl hydroperoxide; the cross section was determined by normalization to the cross section determined using Run 2 data at 10.7 eV.

The mass spectra from the four different pressure data sets provided further information about the product distribution and are shown in **Figure 3-4**. The mass resolution in this data was much improved over the PIE data, but there was a slight shift in the mass calibration so the peaks are ~0.5 amu above their actual masses. The peaks in the figure are all analogous to the ones labeled in the 1 Torr panel. In every case there was a significant peak at m/z 45 when the two dominant peaks were expected to be CH_3CHO and C_2H_5OH. While a ^{13}C and ^{2}H isotope peak of CH_3CHO existed it would

have been a much smaller fraction (~ 2.8%) based on natural abundances. One other feature in **Figure 3-4** is the large m/z 43 peak in the 6 Torr data. It only appeared in this one data set, but it was a signal not a background interference. Other data sets also had one or two unique masses, but only the masses common to every data set have been fully investigated.

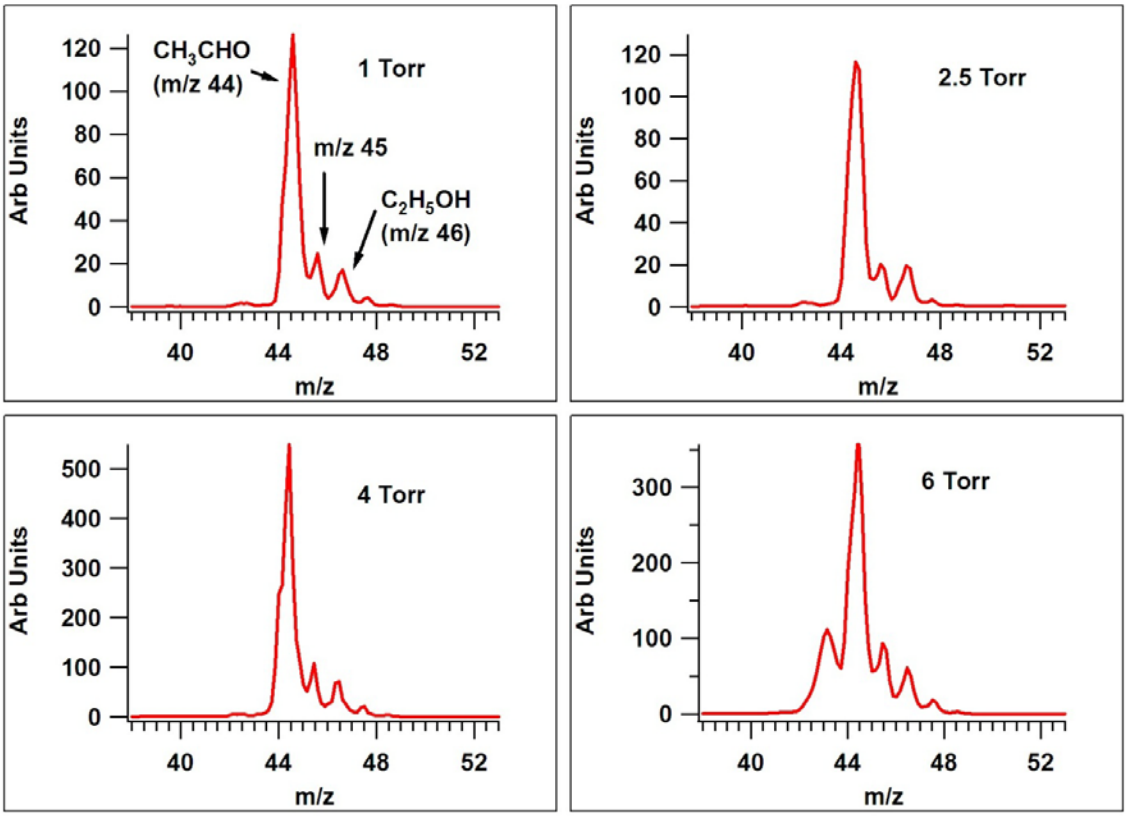

Figure 3-4. 1-D mass spectra of four different pressures; similar peaks are labeled as shown in the 1 Torr panel. m/z 45 peak was much larger than expected based on isotopic abundances. m/z 43 in the 6 Torr panel is also unknown.

The time trace of m/z 45, shown in **Figure 3-5**, looked like a stable product similar to CH_3CHO and C_2H_5OH ruling out a significant radical contribution to the peak. The product at m/z 45 was not the only unexplained product mass. The time traces of some other unexplained masses m/z 105, 89, 60, and 59 are also shown in **Figure 3-5**, and they had clear product time traces as well. Observation of m/z 89 initially suggested

that reaction (3.3) forming diethyl peroxide (m/z 90) may not be negligible. However the m/z 89 product was slower to form than the others indicating that it might have been formed by secondary chemistry and not directly through channel (3.3). In fact there are other isomers at m/z 90 that could explain the observed products including the hemiacetal product in reaction (3.18).

$$CH_3CHO + C_2H_5OH \xrightarrow{surface} CH_3CH(OH)OC_2H_5 \quad (3.18)$$

There was further evidence for this type of chemistry due to a product peak at m/z 105 which may have been the peroxy-hemiacetal (m/z 106) formed from reaction (3.19).

$$CH_3CHO + C_2H_5OOH \xrightarrow{surface} CH_3CH(OH)OOC_2H_5 \quad (3.19)$$

Peroxy-hemiacetal formation is a well known acid and base catalyzed process in organic chemistry. Work from Tobias et al. has seen evidence of this chemistry happening on the surface of aerosols making it possible that the walls of this experiment could provide the surface necessary to catalyze these reactions.[22]

In each case above the predicted masses, 90 and 106, were actually detected at one mass unit lower, i.e., 89 and 105, respectively. This was most likely due to a small mass calibration error at high mass, but another possibility is that both lost H atoms during the ionization. For simplicity they will be referred to as m/z 90 and 106 from here on except in figures where they will be labeled both ways.

The time traces shown in **Figure 3-5** provide clues as to what products might have been linked through dissociative ionization pathways. The initial growth in the time trace of m/z 45 agreed well with the trace at m/z 106 suggesting that the peroxy

hemiacetal might split at the O-O bond after ionization leading to a $C_2H_5O^+$ ion by reaction (3.20).

$$CH_3CH(OH)OOC_2H_5 \xrightarrow{h\nu\ 10.7\ eV} CH_3CH(OH)O + C_2H_5O^+ + e^- \quad (3.20)$$

A companion mass at m/z 60 had a similar time trace indicating that ionized acetic acid and ethanol might also form through reaction (3.21).

$$CH_3CH(OH)OOC_2H_5 \xrightarrow{h\nu\ 10.7\ eV} CH_3COOH^+ + C_2H_5OH + e^- \quad (3.21)$$

The slower appearance of the time trace at m/z 90 did not match well with the time traces of any of the unidentified lower mass products, preventing any clear link from being made. The time trace of m/z 106 and m/z 59 were nearly identical, suggesting that 59 came from 106. The assignment of m/z 59 was not obvious, but might also be linked to the products in reaction (3.21).

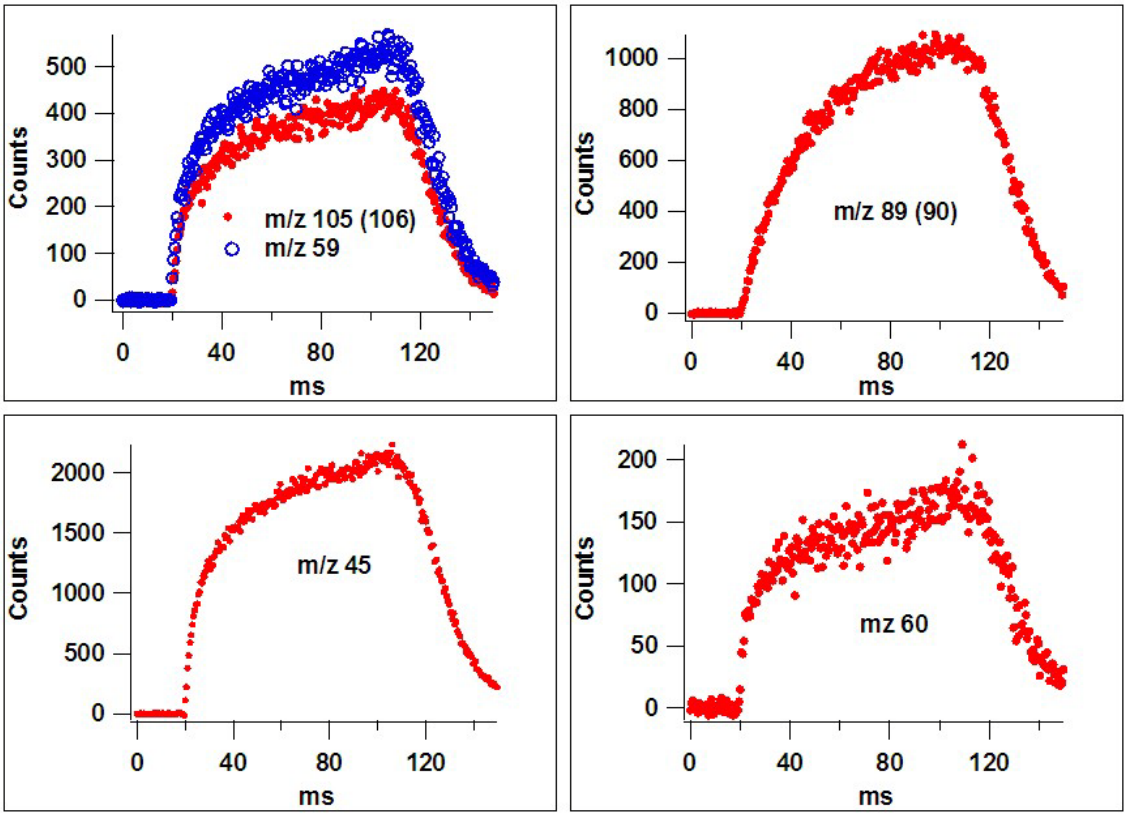

Figure 3-5. Some of the unidentified products and their likely parents at m/z 106 and 90

The PIE curves of these masses also provided information about how they were connected, but it was limited because of the mass contamination already indentified for C_2H_5OH in panel A of **Figure 3-3**. A unique mass must have been present in the PIE of m/z 45 because it appeared well before both acetaldehyde and ethanol as shown in panel A of **Figure 3-6**. Acetaldehyde contamination was subtracted out of the PIE due to its clear interference at around 10.2 eV where it characteristically jumps up. There may have also been ethanol contamination but no subtraction was made. The general curve of the remaining PIE at m/z 45 does not mirror the ethanol PIE, shown in **Figure 3-6** for comparison, and there is no characteristic shape for ethanol that would signal its presence. The best guess PIE for m/z 45 is shown next to the PIE curves from m/z 106, 90, 60, and 59 in panel B. Both m/z 90 and 106 appeared at lower energy than m/z 45, 59,

and 60 indicating that they were possible parents. In the inset of panel B it is shown that m/z 45 and m/z 60 have very similar appearance energies. This is in agreement with the time traces that suggested dissociation channels (3.20) and (3.21) were complimentary. In addition m/z 60 appeared well before the known appearance energy of acetic acid at 10.6 eV, so m/z 60 could not be attributed to acetic acid formed through other chemistry.[23] The appearance of m/z 59 did not happen until higher energy indicating a different pathway was needed for its formation.

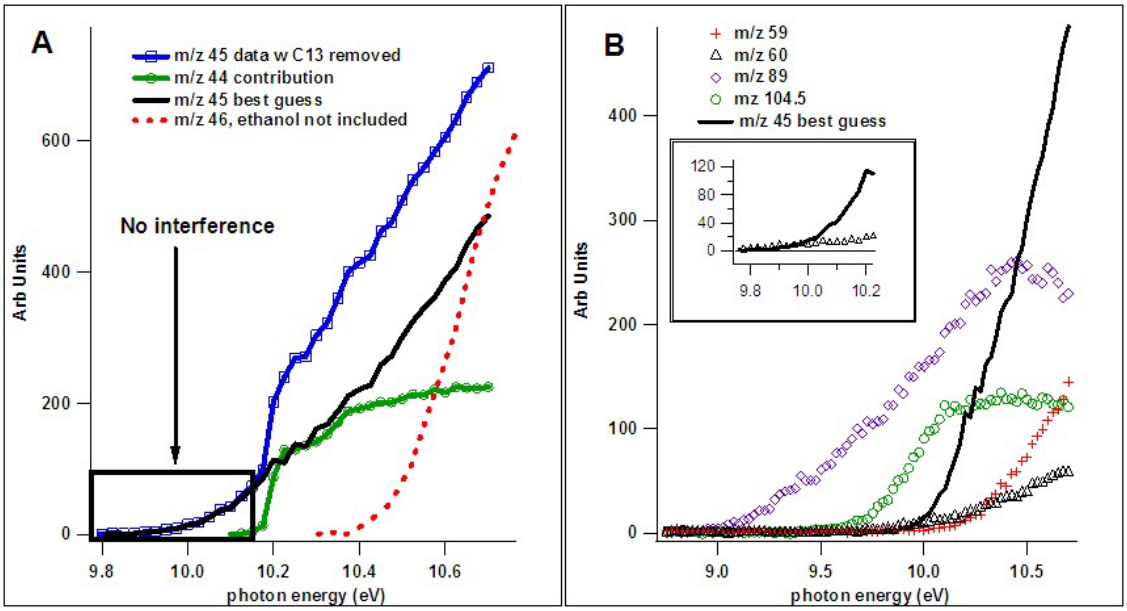

Figure 3-6. (A) Removing acetaldehyde mass contamination from m/z 45 PIE. Ethanol was not removed, but is shown for comparison. (B) A comparison of the PIE curves for the larger masses and some of their possible dissociation products.

Table 3-1 lists all of the reproducible masses observed and their species assignments where possible. Description explains whether the species time trace looked like a reactant, product, or a step function (e.g., a product that comes up almost instantly at the firing of the excimer due to its formation from the initiation chemistry, but is neither created nor destroyed in the subsequent reactions). Two species which have not already been mentioned are butene (C_4H_8) and butane (C_4H_{10}). Both had time traces

indicating initial formation at the firing of the excimer, but then no further reaction. Recombination of C_2H_5 radicals may have been the source of one or both species. The butene PIE was not in exact agreement with the PIEs in the literature so some doubt in this assignment remains.[18,24] An excited $(CO)_2^+$ from OxCl photolysis might also appear at this mass. Butane did not appear in the PIE data set because of insufficient signal-to-noise, but it has an appearance energy of 10.53 eV and so would have been observed during the kinetics data sets at 10.7 eV where much more averaging was done.[18]

Table 3-1. All the reproducible masses identified in Runs 1A and 2 as well as their species assignment and a description of how their time trace appeared.

Run 1A (m/z)	Run 2 (m/z)	Species	Description
28	28	$C_2H_4^+$	Step function
29	29	$C_2H_5^+$ (from $C_2H_5O_2^+$)	Reactant
44	44	CH_3CHO^+	Product
45	45	$C_2H_5O^+$ (From dissoc) And $^{13}C/^2H$	Product
46	46	$C_2H_5OH^+$	Product
47	47	? And $^{13}C/^2H$	Step function, small product
56		$C_4H_8^+$	Step function
58		$C_4H_{10}^+$	Step function
59		? (From dissoc)	Product
60		CH_3COOH^+ (From dissoc)	Product
62	62	$C_2H_5OOH^+$	Product
89 (90)	89 (90) sometimes	$C_2H_5OOC_2H_5$ or $CH_3CH(OH)OC_2H_5$	Product
105 (106)		$CH_3CH(OH)OOC_2H_5$	Product

3.3.1.1.b Measurement of α

Using the assigned product masses the simplest way to measure α was to use equations (ii) and (iii); determining *R* from the ratio of the CH_3CHO and C_2H_5OH time profiles. **Figure 3-7** shows a plot of the time trace of *R*. In each case a stable ratio was

reached after ~ 20 ms validating the steady state approach used. The results spanned the range α = 0.52 – 0.58.

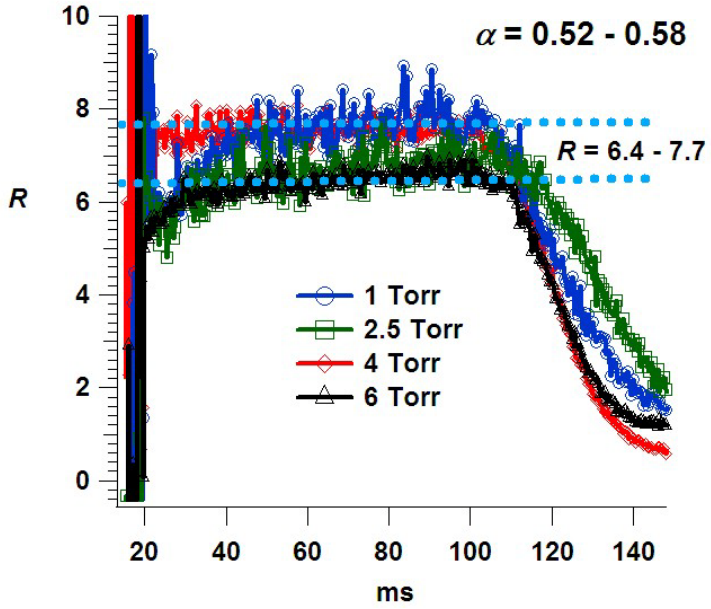

Figure 3-7. Ratio of CH_3CHO counts to C_2H_5OH counts and value for α that was determined from the ratios at the four pressures 1, 2.5, 4, and 6 Torr.

As shown in **Figure 3-2**, α was also measured by performing kinetics fits to the time traces using the calibration factor to determine absolute concentrations. This method agreed well with the *R* method. The calibration factor was not well known (the slits on the micrometer were changed during the calibration run leading to an unknown amount of photons) so the absolute kinetics were uncertain, but the relative nature of α meant that the fitted parameter was robust no matter what calibration factor was used to translate counts into concentration. (e.g., The total self reaction rate constant for one data set varied over the range 9.65 x 10^{-14} – 3.07 x 10^{-13} cm^3 $molecules^{-1}$ s^{-1}, using a calibration factor that also varied by a factor of three, but α only varied over the range 0.532 – 0.579)

3.3.1.1.c Other product ratios: $R_{A/EH}$ and $R_{E/EH}$

The other ratios $R_{A/EH}$ and $R_{E/EH}$ provided more information about the progress of the reaction. **Figure 3-8** shows both ratios, neither was constant in time and both increased prior to the pump out that started at ~ 100 ms. From the ratios it was especially clear that the products were not pumping out at the same rate. $R_{A/EH}$ got much smaller throughout the pump out showing that CH_3CHO was being removed the fastest, and $R_{E/EH}$ got much larger showing that C_2H_5OH was removed the slowest. There were also changes in the ratios with pressure, but this was expected. The branching fraction between reaction (3.6) and reaction (3.7) is pressure dependent, so the initial amount of C_2H_5OOH will also be pressure dependent. Without knowing the photoionization cross section a value for α can not be independently determined from this data.

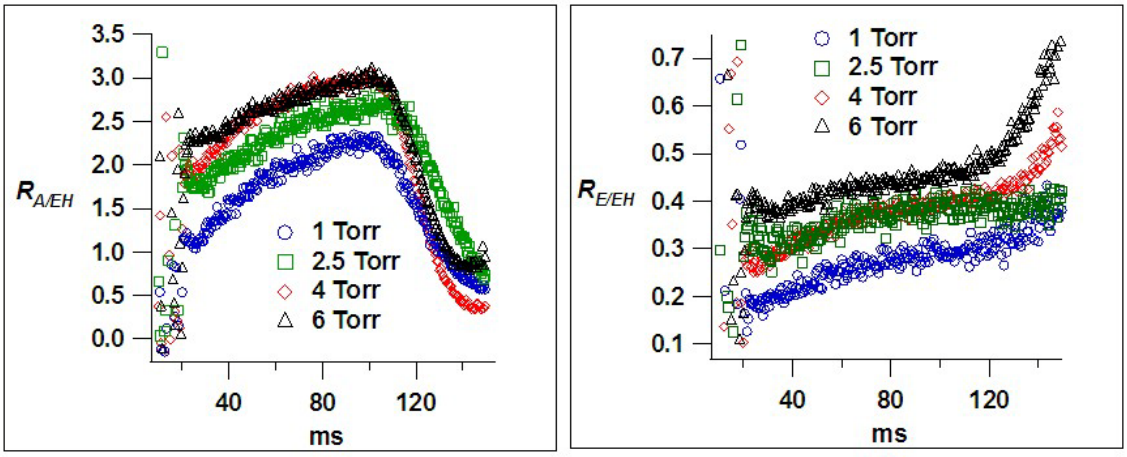

Figure 3-8. Ratios of [CH_3CHO] / [C_2H_5OOH] and [C_2H_5OH] / [C_2H_5OOH] in the left and right panels respectively. Behavior during the pump out shows that the products had different retention in the flow cell.

3.3.1.2 Run 1B (DEK chemistry)

The DEK precursor chemistry was also tried during Run 1. The total radical concentration was ~ 1 order of magnitude lower than the OxCl chemistry in Run 1A, largely due to the smaller photolysis cross section of DEK. The DEK chemistry was an interesting comparison because Cl was not needed due to the direct production of ethyl

radicals from photolysis. A strange distribution of products meant that a measurement of α was not reliable.

3.3.1.2.a Observed Products

The reactants and products, C_2H_5, CH_3CHO, C_2H_5OH, and C_2H_5OOH shown in **Figure 3-9**, were observed during the DEK data sets. The time traces did not all have the same shape. The C_2H_5 had a sharp initial drop followed by a slower reaction that looked like the $C_2H_5O_2$ self reaction. C_2H_5OH counts jumped up very quickly and then only increased marginally for the rest of the reaction time. The C_2H_5OOH appeared to form a little bit more slowly than everything else. Only the CH_3CHO has the characteristic time trace expected. In addition the amount of C_2H_5OOH was also quite large, nearly equaling the CH_3CHO trace, but during the OxCl chemistry in Run 1A CH_3CHO was ~ 3 times greater than the C_2H_5OOH. The data shown here are for the 6 Torr data but similar results were obtained for the 4 and 1 Torr data sets, albeit with lower signal-to-noise ratios.

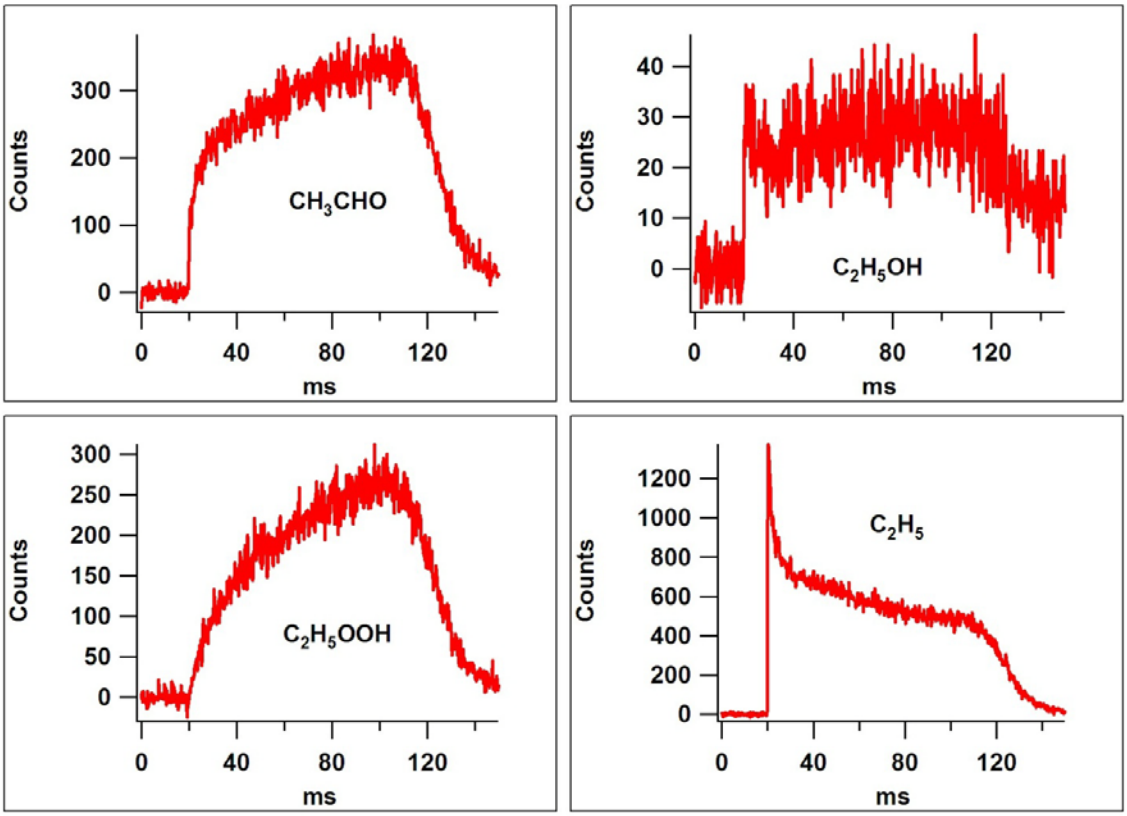

Figure 3-9. Expected products and reactants of $C_2H_5O_2$ self reaction using the DEK precursor chemistry. Time traces do not all appear the same, and are different from the behavior they showed in the OxCl chemistry.

The results from the DEK chemistry also had unexplained mass peaks. **Figure 3-10** shows the mass spectrum from the 6 Torr data set. The peaks at m/z 45 and 47 were as large or larger than the C_2H_5OH peak at m/z 46. Their time traces are shown in the next panel where m/z 47 appeared as a step function, and m/z 45 grows in as a product after an early transient peak. Both of these peaks well exceed what would be expected from natural isotopic abundances. There was also a new prominent peak at m/z 42 which reacted away with time. It was not possible to look for the larger mass products (m/z 90 and 106) because the ion optics were tuned so that anything larger than DEK (m/z 86) would not hit the detector to avoid saturation from the DEK signal. This made it hard to determine whether the unexpected mass peaks came from a larger parent. No PIE data

was taken with this chemistry so it was not possible to identify the products that way either. A data set was taken that verified photodepletion of the DEK signal before it was tuned off the detector, and indicated there was a good photolysis laser alignment.

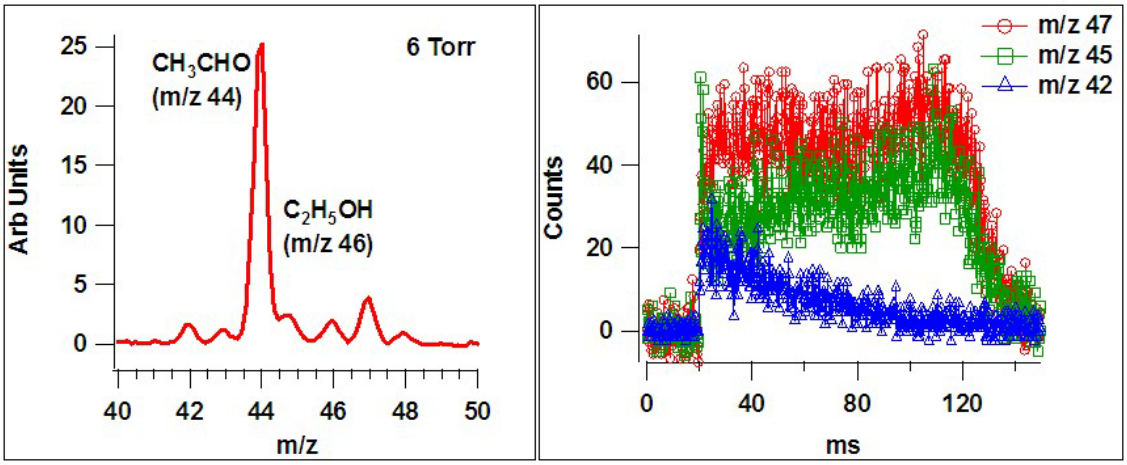

Figure 3-10. 1-D mass spectrum from DEK chemistry, and time traces of selected masses

3.3.1.2.b Measurement of α

The strange mass distribution around the critical product masses combined with low signal-to-noise from the lower radical concentration meant that α from this data was not reliable. This data was not considered for the overall measurement of α for the $C_2H_5O_2$ self reaction.

3.3.1.3 Run 2

In Run 2 the OxCl chemistry at ~ 1 order of magnitude lower radical concentrations (~ 1 x 10^{13} molecules cm^{-3}) was explored. One data set was also taken to determine if changing the O_2 concentration would have an effect. Good measurements of α were made with few unknown product masses observed.

3.3.1.3.a Observed Products

The product masses CH_3CHO, C_2H_5OH, C_2H_5OOH, and C_2H_4 were all observed and are shown in **Figure 3-11**. The C_2H_5 reactant trace also was observed as expected. In

this OxCl run the product masses all pumped out at the same time unlike during Run 1A. The product time traces have similar qualitative shapes except for the CH_3CHO which appeared to jump up earlier. No PIE was taken during this run so the species assignments from Run 1A were used.

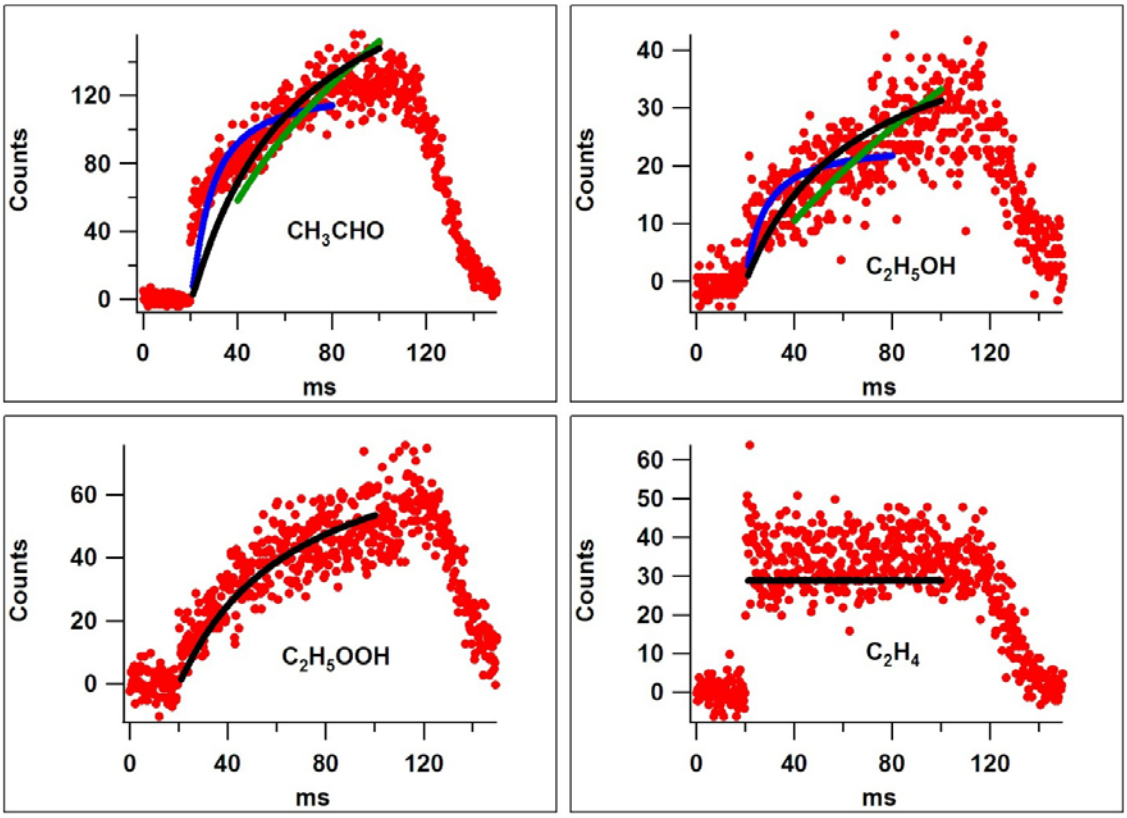

Figure 3-11. Stable products from the 6 Torr, 248 nm, high O_2 data set in Run 2. Different time scale fits are shown, as well as when the fit to ethyl hydroperoxide is included along with an initial HO_2 constraint from the ethene.

In **Figure 3-12** the mass spectrum of each data set around m/z 40 is shown. Clear resolution of the individual peaks was seen. The peaks at m/z 45 and 47 were much smaller than the expected product peaks at m/z 44 and 46. They were still not quite as small as would be expected from isotopic abundances, but with careful removal of the tails of the neighboring peaks they are only slightly larger. The time trace of m/z 45 is not shown but still resembled a stable product. Comparing the top two panels shows no

observable difference between flash photolysis at 193 nm and 248 nm. There was also no qualitative difference from the addition of extra O_2 as can be seen by comparing the bottom two 6 Torr panels. The quantitative differences will be discussed shortly.

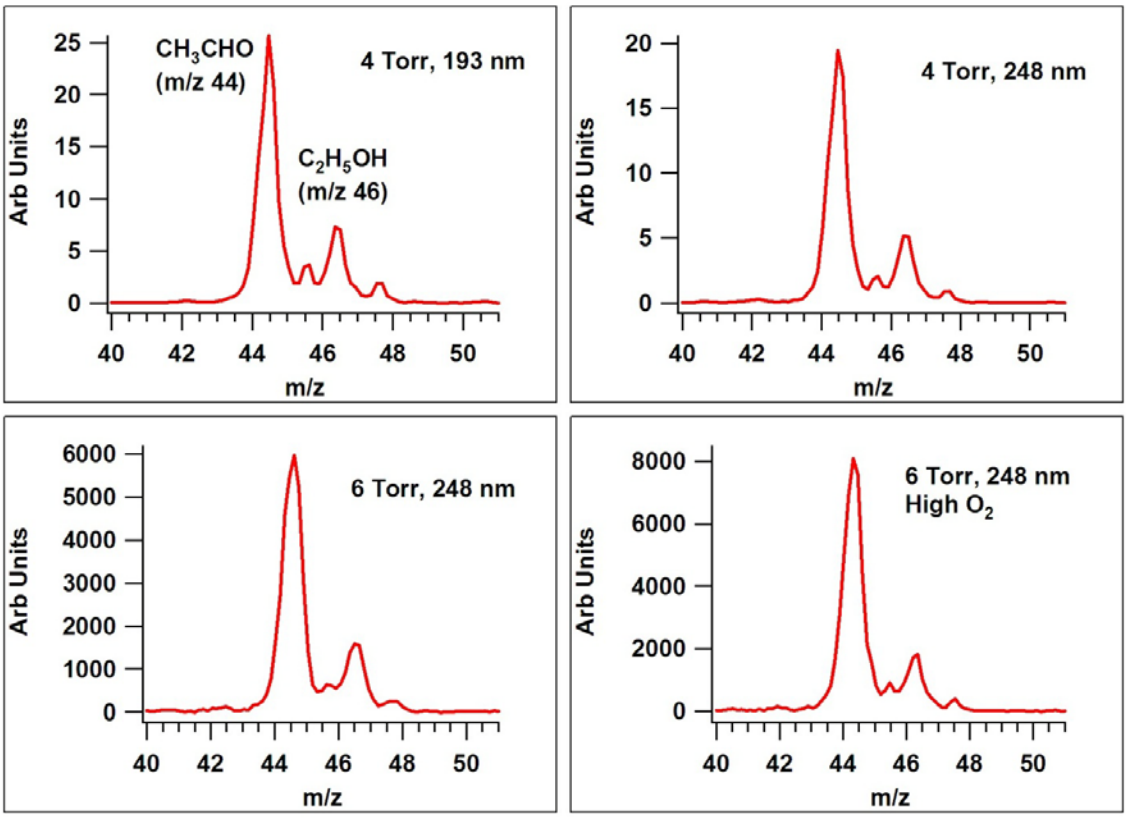

Figure 3-12. 1-D mass spectra in the m/z 4X range from the four data sets taken during Run 2. All the peaks are labeled analogously to the first panel. m/z 45 and 47 are much smaller than m/z 44 and 46, as expected.

There were not as many additional masses observed during Run 2. The product at m/z 90 was not conclusively observed in every run. **Figure 3-13** shows the observed time traces for m/z 90 for the four different data sets. The 6 Torr data in the bottom two panels was taken last and no m/z 90 was observed. The variable nature of the detection makes it likely that it resulted from a secondary process. There was also no detection of m/z 106 in any of the data sets from Run 2. **Table 3-1** lists all of the observed masses during Run 2 in comparison with all of the observed masses from Run 1A.

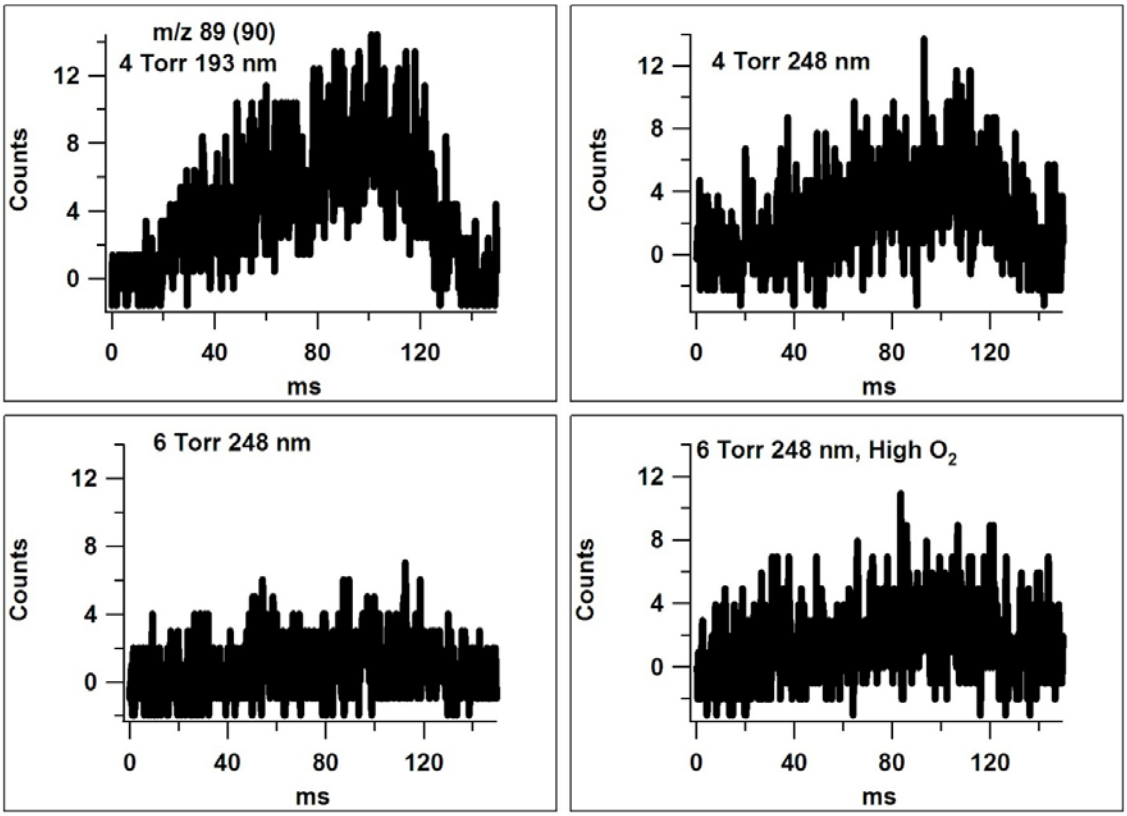

Figure 3-13. m/z 90 was not observed in every data set. The sporadic detection indicated that it was likely a secondary product, not one produced in the $C_2H_5O_2$ self reaction.

3.3.1.3.b Measurement of α and O_2 dependence

Similar to Run 1A, α was determined by both kinetic fitting and looking at *R*. The kinetic fits are plotted with the time traces in **Figure 3-11**. In all the kinetics fits shown the value for α did not change substantially despite the clear differences in the fits. The blue and green fits were done over different time ranges, and the black fits included the C_2H_5OOH and C_2H_4 data as well. As in Run 1A the rate constant values were too large, ~ 3 x 10^{-13} cm^3 $molecules^{-1}$ s^{-1}, to be considered realistic using the concentration factors derived from the calibration gas data set. The relative nature of α meant that it did not depend on these concentration factors as previously discussed for Run 1A. The value for

α from the kinetics fits is 0.34 ± 0.06. The value was determined as an average of all four data sets and the quoted errors are the standard deviation of those measurements.

The signal-to-noise for these data was lower than in Run 1A (predominantly due to the lower radical concentration), and was especially evident when looking at *R* as shown in **Figure 3-14**. It was less clear cut what should be taken as the value for *R*, so a linear fit was performed over the time range 60 – 100 ms, (the area inside the pink box) and the average value of the linear fit was taken for *R*. The average of the four data sets leads to α = 0.33 ± 0.08, where the quoted errors are the standard deviation of the four measurements. The values for α obtained from the kinetics fits and *R* for each individual data set are shown in **Table 3-2**. The individual errors for α from *R* were determined by taking the high and low *R* value determined from the linear fit just described, and the error from the kinetics fitting was determined by the range of α determined in the different types of fits.

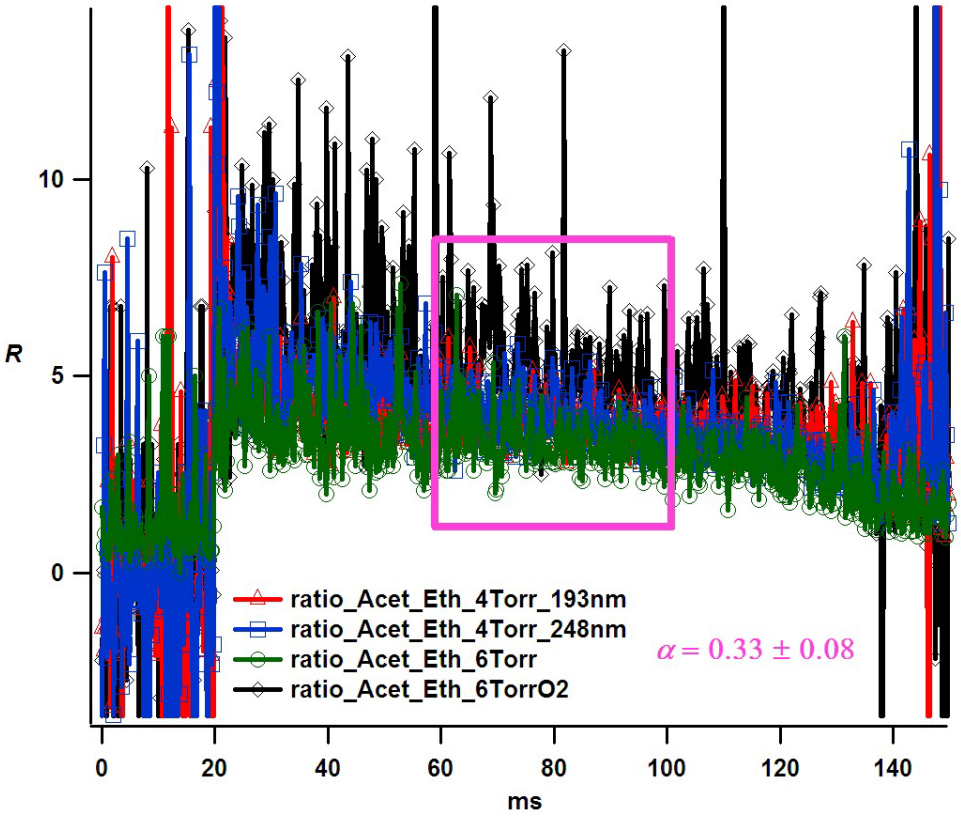

Figure 3-14. *R* plotted for the four data sets of Run 2. The area within the pink box (60–100 ms) is the region used for determining the *R* and the corresponding α for each data set. The average value for α determined is also stated in pink.

The O_2 dependence of this reaction was also investigated with the two data sets at 6 Torr. Competition from reaction (3.8) might have interfered with the end product analysis at low O_2 concentrations so a higher O_2 concentration was also tried at 6 Torr. The value for α does change with the addition of extra O_2 as can be seen in **Table 3-2**. The additional O_2 in the carrier gas led to lower signal-to-noise making it difficult to determine how robust this effect was with only the one data set including the variation. This signal-to-noise effect was evident in the initial radical determined in **Table 3-2** for the high O_2 run. Nothing except the O_2 concentration was changed from the previous run but using a similar calibration factor returned an initial radical concentration a factor of two lower. In reality (and in parenthesis for Img_020) the radical concentration would

have been approximately the same as the previous run, but the extra O_2 led to less of the sample from the pinhole making it into the ionization region of the instrument.

Table 3-2. Conditions and α values measured for each of the data sets in Run 2

Run	P (Torr)	Laser (nm)	# of Shots	$[C_2H_5]$ / 10^{13}	$[O_2]$ / 10^{16}	α from R	α from kinetics
Img_014	4	193	2000	2.8	1.3	0.31 ± 0.03	0.28 ± 0.02
Img_018	4	248	7500	1.1	1.3	0.32 ± 0.03	0.32 ± 0.02
Img_019	6	248	3750	1.0	1.3	0.24 ± 0.06	0.31 ± 0.02
Img_020	6	248	3750	0.45 *(1.0)*	4.9	0.43 ± 0.06	0.42 ± 0.02

3.3.1.3.c C_2H_5OOH photoionization cross section

The kinetics fits in black in **Figure 3-11** that included the C_2H_5OOH and C_2H_4 data were also used to determine the photoionization cross section of C_2H_5OOH relative to the other products. The C_2H_4 data constrained the initial amount of C_2H_5 radicals and the initial amount of HO_2 through the known branching ratio between reaction (3.6) and (3.7). The α value measured from CH_3CHO and C_2H_5OH determined the additional amount of secondary HO_2. Assuming that C_2H_5OOH only forms through reaction (3.5) a determination of the C_2H_5OOH cross section for the data was then possible because the absolute concentrations of all the sources of C_2H_5OOH were known. The photoionization cross section at 10.7 eV was determined to be 2.57 Mb. This measurement was then used to scale the PIE curve taken in Run 1A to provide cross sections for the range 8.6 – 10.7 eV. The error on this measurement will be discussed further in the discussion section.

3.3.1.3.d Other product ratios: $R_{A/EH}$ and $R_{E/EH}$

The other ratios, $R_{A/EH}$ and $R_{E/EH}$, were also looked at for Run 2, and are shown in **Figure 3-15**. The ratios showed the same overall shape starting out larger before settling at a plateau. While both CH_3CHO and C_2H_5OH pumped out more quickly than C_2H_5OOH the change was not as dramatic as in Run 1. It was possible to check for self consistency in the data by using the photoionization cross section derived from this data to determine α from these ratios. This was complicated by the fact that a large amount of the C_2H_5OOH in this data comes from the initial HO_2 formed in reaction (3.7). After a best guess subtraction of the initial C_2H_5OOH the data was used to determine α, and consistency within the results was observed.

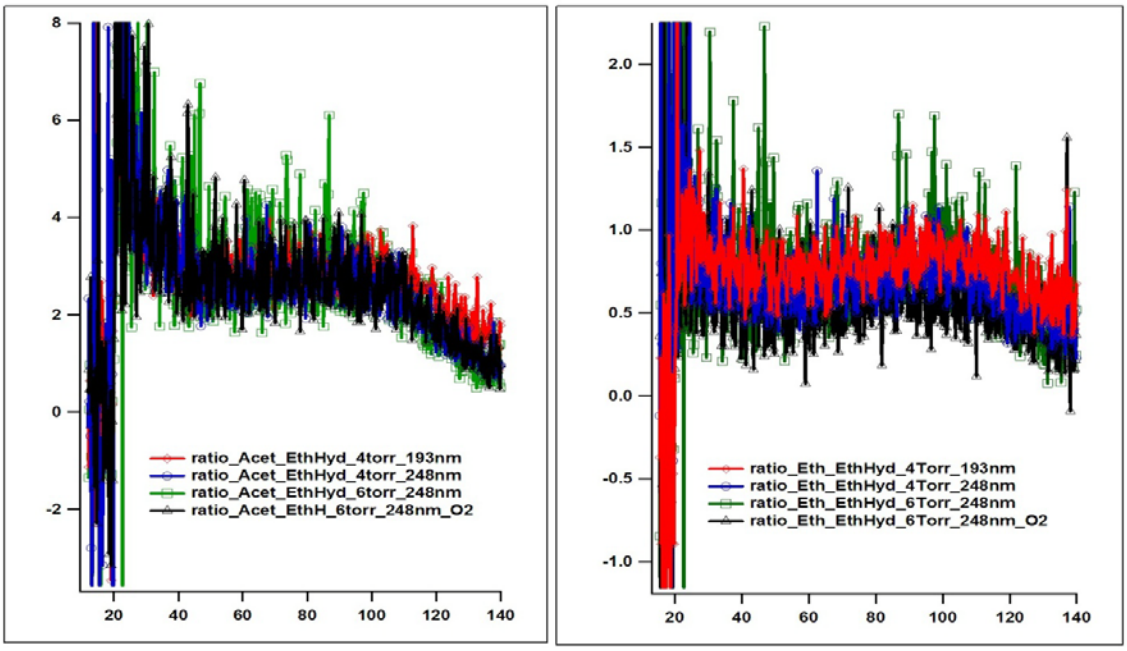

Figure 3-15. The ratio of CH_3CHO/C_2H_5OOH and C_2H_5OH/C_2H_5OOH for the four data sets in Run 2

3.3.1.3.e Differences in radical concentration

The absolute concentrations have been checked by comparing the OxCl depletion at 11.1 eV and determining a total Cl concentration of 3.3 x 10^{12} molecules cm^{-3} for the 193 nm photolysis runs. This was almost an order of magnitude lower than the value of

2.8×10^{13} estimated from the concentration of C_2H_4 observed and assuming a branching fraction of 0.13 for reaction (3.7).[25,26] The reason for this discrepancy was unknown, but the observed rate of reaction was consistent with the higher concentrations determined from the calibration factor, suggesting that more OxCl may have been present than expected.

3.3.1.4 Run 3

The main goal of this run was to further investigate the role that O_2 and total radical concentrations have on the measured value of α. It was discovered too late that problems with the experimental apparatus had led to unusable data sets. **Figure 3-16** shows the mass resolustion from around the main product peak m/z 44 and 46 for four data sets during Run 3. It was not possible to make a clear distinction of each mass so it was not possible to determine the appropriate ratio. Individual shift corrections (the alignment of counts from alike masses that appear curved in the raw data) were done for each data set, but this did not improve the data significantly. For now this data has not been used.

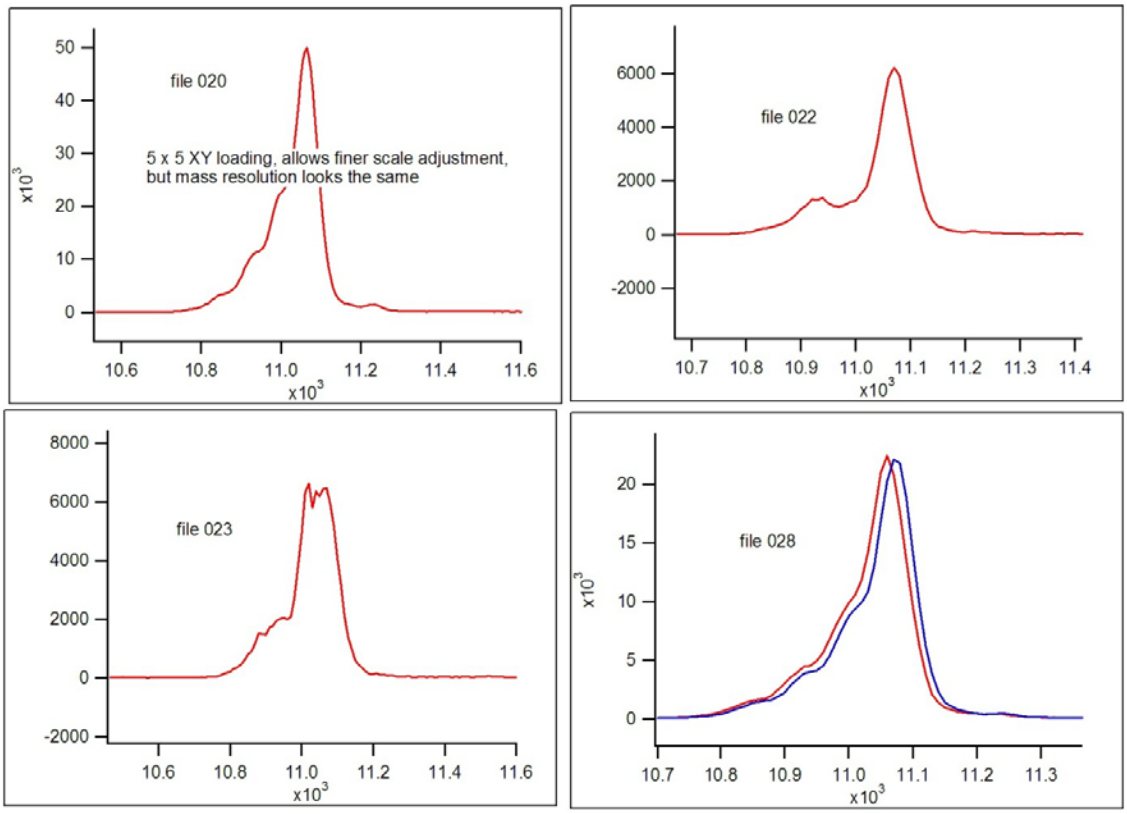

Figure 3-16. The mass resolution in the 4X range for Run 3 is very poor, as shown in four different data sets.

3.3.2 CH_3O_2 self reaction

Acetone photolysis was used as the precursor chemistry for the CH_3O_2 self reaction. The expected products were identified, and a preliminary measurement of α was made using one 4 Torr data set with sufficient signal to noise. More data is needed to confirm the value.

3.3.2.1 Observed Products

The major products formaldehyde (HCHO), methanol (CH_3OH), and methyl hydroperoxide (CH_3OOH) were all observed and are shown in **Figure 3-17**. In addition the reactant methyl peroxy (CH_3O_2) itself was observed, unlike in the case of ethyl or propyl, because it has a stable cation at m/z 47 and does not dissociatively ionize until

higher energies.[27] There was an interference at m/z 32 which was visible in the CH_3OH signal as a transient species very early in the time trace. A small sulfur contamination from the previous run may have been responsible. The pump out portion of all the time traces looked similar as well. The 1 Torr data set is not shown, but looked qualitatively the same although it had much poorer signal-to-noise.

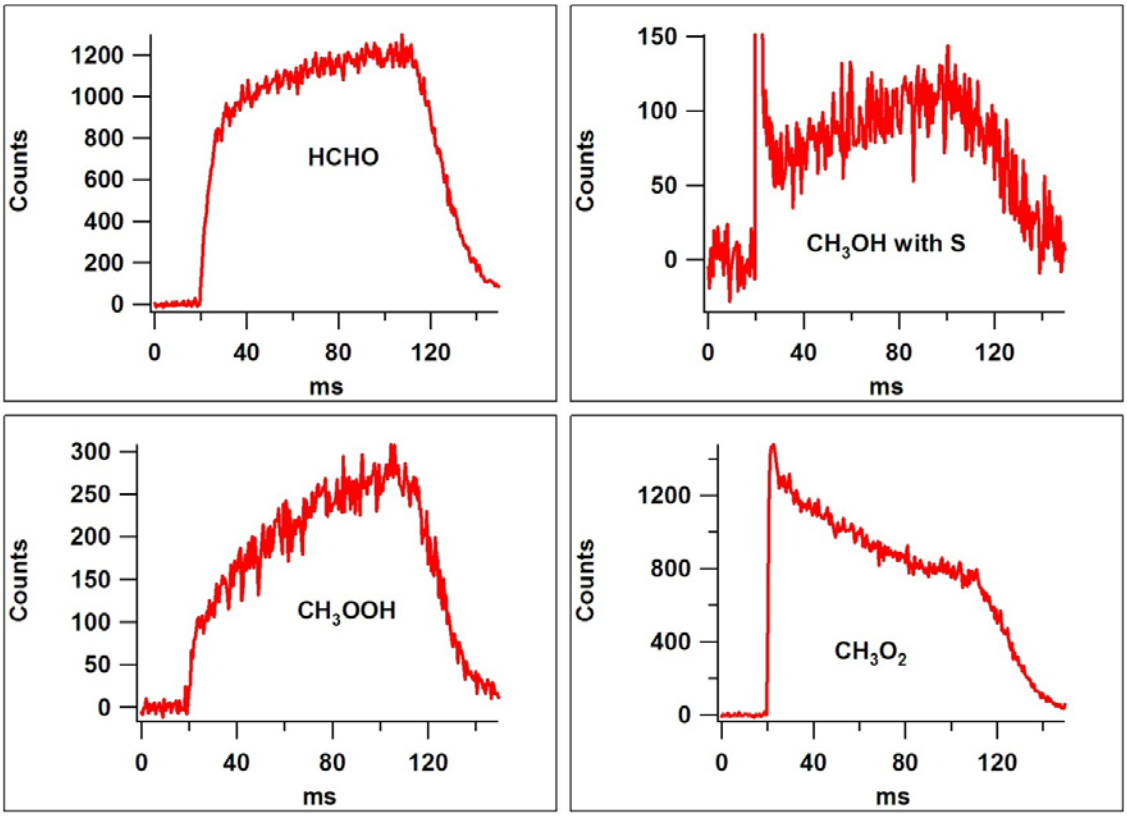

Figure 3-17. The three major products – HCHO, CH_3OH, and CH_3OOH – along with the reactant CH_3O_2 from the methyl peroxy self reaction.

The products were confirmed by their PIE scans and comparison to the literature where possible. Absolute cross sections were not measured, but the PIEs were normalized to the literature value of the cross section at 11.4 eV for comparsion of the overall shapes shown in **Figure 3-18**. There was good agreement between the qualitative shape from the present measurement of HCHO and CH_3OH and the work of Cooper et al. and Cool et al., respectively.[15,16] There are no previously reported PIE curves for CH_3OOH, but from

photoelectron spectroscopy Li et al. report a first ionization energy of 9.87 eV.[21] We did not measure low enough in energy to confirm this measurement, but at 10.0 eV the signal was not quite extinguished suggesting that the first ionization is < 10.0 eV. There are no previously reported cross sections for CH_3O_2 either, but the PIE curve measured here was in good agreement with previous work from the same instrument.[27]

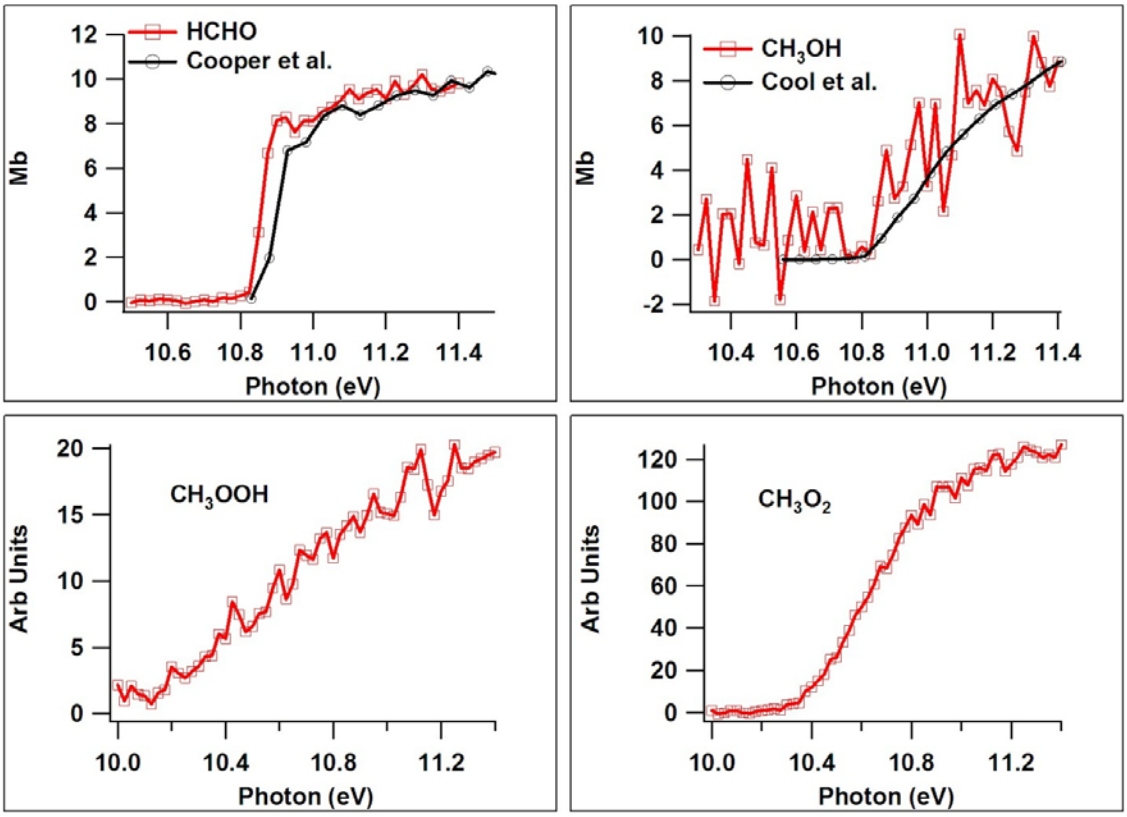

Figure 3-18. PIE scan of major reactants and products of CH_3O_2 self reaction. Absolute cross sections were not measured, but scans were normalized to literature value at 11.4 eV for comparison where possible.

There was good mass resolution for these data sets as is shown in panel A of **Figure 3-19**. The small peak at m/z 31 between HCHO and CH_3OH has a magnitude corresponding to the expected isotope ratio of HCHO. A depletion was observed as expected at the CH_3CO fragment from dissociative ionization of the acetone precursor. Masses larger than m/z 58, where the precursor acetone was found, could not be reliably

measured because the ion optics were adjusted to move m/z 58 to the edge of the detector to prevent signal saturation.

3.3.2.2 Measurement of α

For the CH_3O_2 self reaction R = [HCHO]/[CH_3OH]. Unfortunately only the data taken at 4 Torr had sufficient signal-to-noise to determine α so only the one measurement shown in panel B of **Figure 3-19** was made. From this data $\alpha = 0.53 \pm 0.03$.

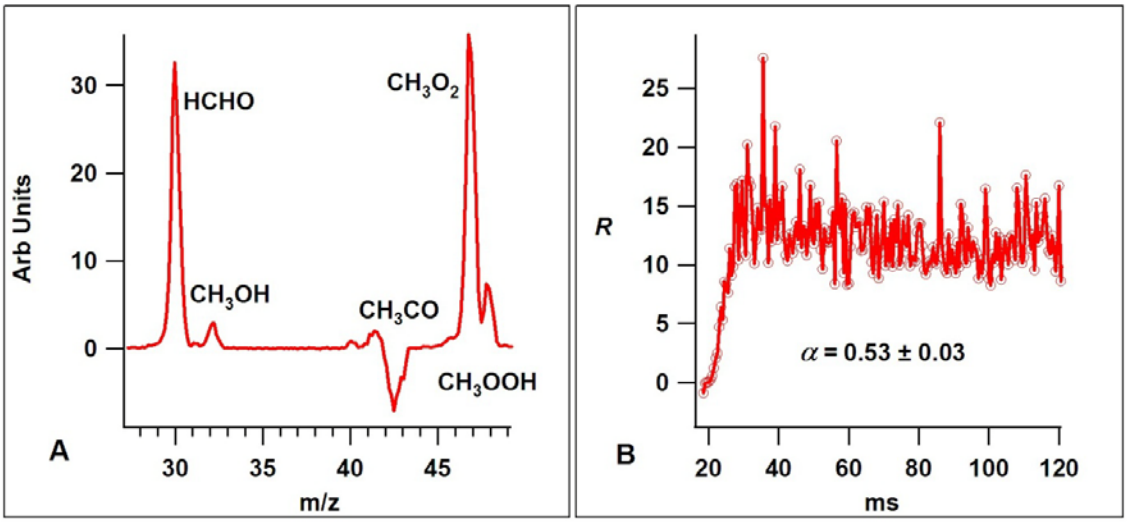

Figure 3-19. A. Mass resolution of the major reactants and products was good. B. R = [HCHO]/[CH_3OH] for the CH_3O_2 self reaction and allowed measurement of α.

3.3.3 $C_3H_7O_2$

Both OxCl and DPK chemistries were used to generate $C_3H_7O_2$ radicals, and both had problems with product identification. The OxCl chemistry also had high molecular weight species and differing pump out traces for different products. Neither chemistry provided a reliable measurement of α.

3.3.3.1 Run 1A (OxCl chemistry)

3.3.3.1.a Observed Products

The results from the OxCl chemistry for the $C_3H_7O_2$ self reaction show the expected major products and reactants. **Figure 3-20** shows the time traces for the carbonyl (C_2H_6CO) , alcohol (C_3H_7OH), hydroperoxide (C_3H_7OOH) and propyl radical (C_3H_7) from the dissociative ionization of propyl peroxy ($C_3H_7O_2$). The pump out portion of the time traces for C_3H_7OH and C_3H_7OOH were very different from the C_2H_6CO and the C_3H_7. Over the time period observed there was almost no removal of the former compared with almost complete removal of the latter. The data shown is for the 6 Torr data set, but the 4 Torr and 1 Torr data also mimicked this behavior.

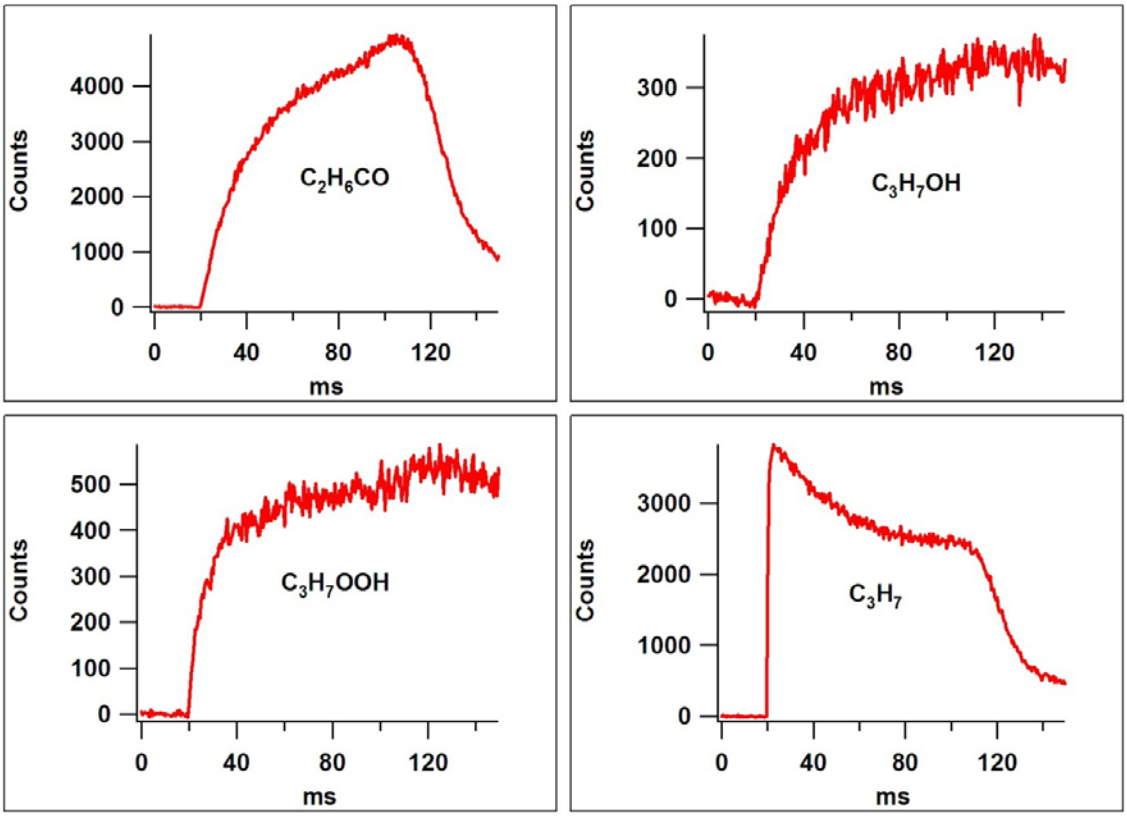

Figure 3-20. Major products and reactants for $C_3H_7O_2$ self reaction using the OxCl precursor chemistry.

Identification by PIE was more complicated in this case because both C_2H_6CO and C_3H_7OH were most likely a combination of isomers from the two different propyl peroxy radicals. The C_2H_6CO (m/z 58) PIE could be reasonably well reproduced by a

10:1 mixture of the propanal and acetone PIE curves as shown in **Figure 3-21**. Another way to determine the acetone contribution would have been through its dissociative ionization at m/z 43. However whatever product signal may have been there was swamped by the dissociative ionization of the reactant $C_3H_7O_2$, as can be seen in the reactant time trace in **Figure 3-20**. The identification of m/z 43 as C_3H_7 was further confirmed by the PIE curve which started well before 10.3 eV, the beginning of the dissociative ionization of acetone. It was not possible to get as good agreement for the C_3H_7OH (m/z 60) PIE curve by combining the PIE curves of 1 and 2-propanol. The data appeared at lower energy than either alcohol isomer indicating a possible mass contamination from another source. At higher energy the upward curvature strongly suggested the presence of at least 1-propanol. There is no literature data for C_3H_7OOH, but the PIE resembles that of CH_3OOH and C_2H_5OOH (first I.E. 9.87 and 9.65 eV, respectively)[21], and with an appearance energy of ~ 9.6 eV it followed the trend of decreasing appearance energy with larger alkyl group.

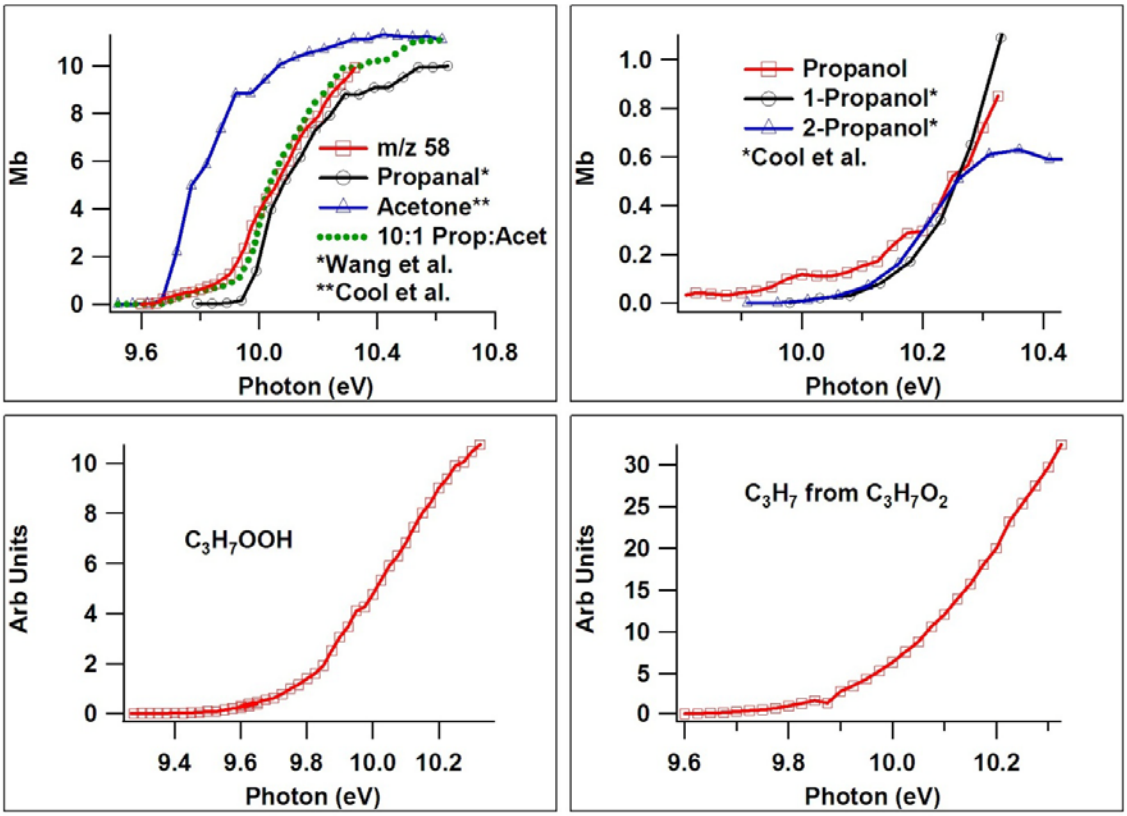

Figure 3-21. PIE of major products and reactants from $C_3H_7O_2$ self reaction using OxCl precursor chemistry.

There were additional masses of interest using this chemistry, some similar to those seen in Run 1A of the $C_2H_5O_2$ work. There was a significant product mass at m/z 44, and from the time trace and PIE curve shown in **Figure 3-22** it appeared that it was largely acetaldehyde. A contribution from dissociative ionization of 2-propanol could not be ruled out, and it was not clear why the appearance energy appeared shifted to lower energy. Also in **Figure 3-22** CH_3O_2 was clearly observed and so was a product at m/z 120. The mass calibration at as large a mass as m/z 120 may have not been accurate, and this product may be the hemi-acetal formed from the reaction of propanal with 1-propanol at m/z 118.

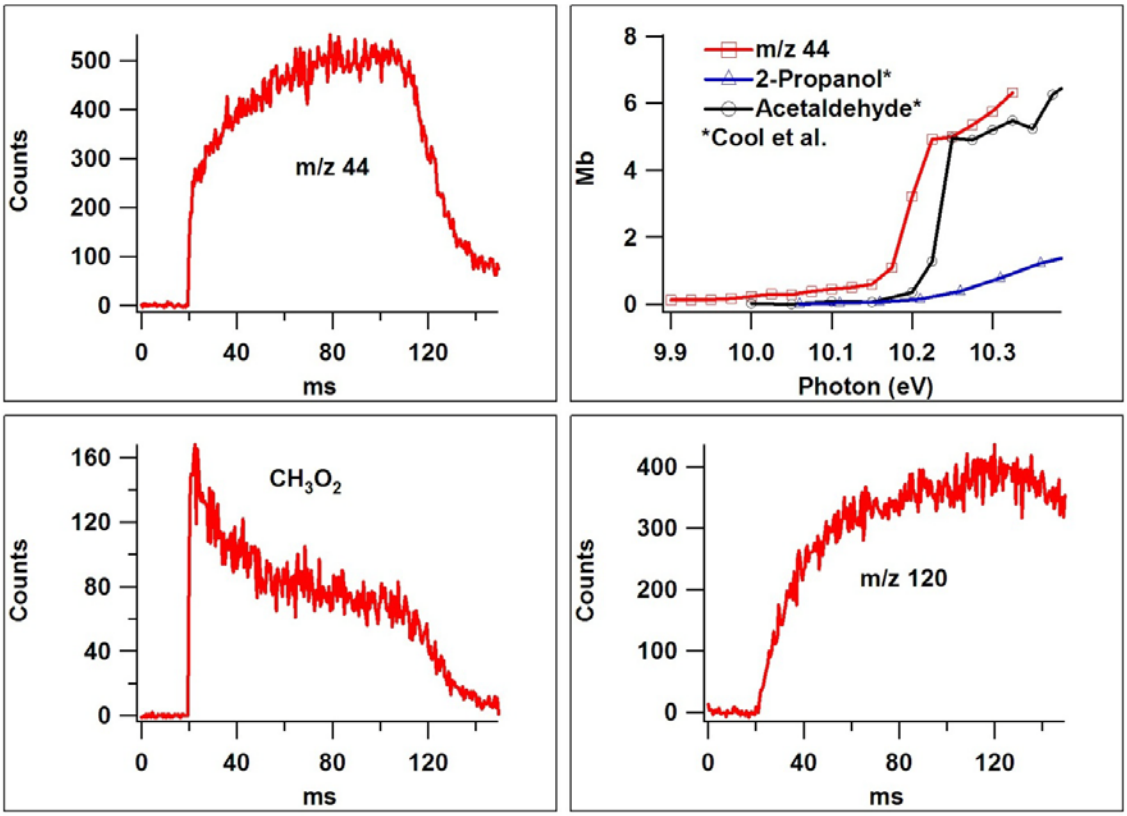

Figure 3-22. Other masses of interest from the propyl peroxy reaction using OxCl precursor chemistry.

3.3.3.1.b Measurement of α

The inability to confidently determine the species asignments at the expected product masses made it impossible to determine α. A more definitive PIE measurement would allow determination of the amount of each product, as would a combination of single point runs at energies that would select for one or other isomer.

3.3.3.2 Run 1B (DPK chemistry)

3.3.3.2.a Observed products

The DPK precursor chemistry was used to avoid the isomer problems of the OxCl precursor chemistry. It was surprising when all the major products were not observed. There was no evidence of C_3H_7OH at m/z 60 as shown in **Figure 3-23**. There was also an

interesting correlation between the rapid rise in C_2H_5CHO and the rapid decline in C_3H_7 both of which qualitatively appear to occur faster than the $C_3H_7O_2$ self reaction.

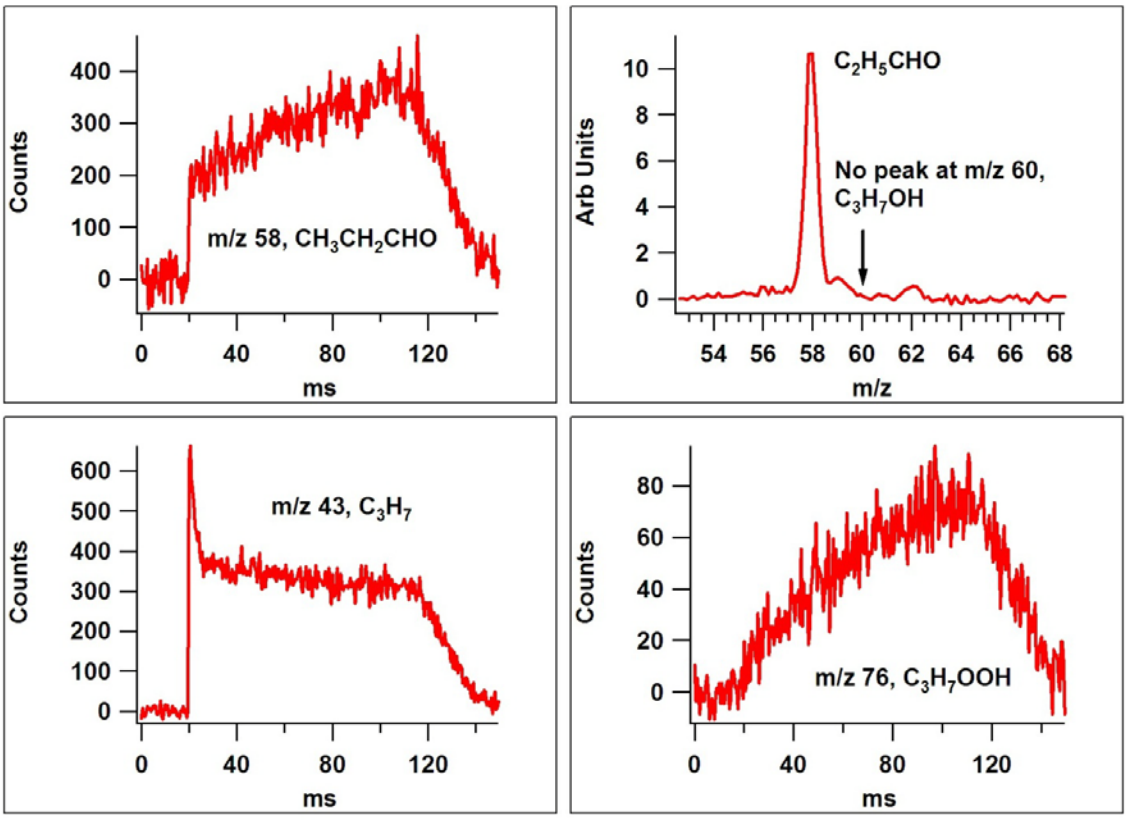

Figure 3-23. Major products and reactants using the DPK chemistry for propyl peroxy.

The PIE curves for these products shown in **Figure 3-24** also left some uncertainty as to their exact assignment. C_2H_5CHO still had the early appearance energy that it had in the OxCl chemistry, making it appear that acetone was contributing as well. The inclusion of acetone still did not resolve the mismatch at higher energies between the PIE curves, suggesting some unknown chemistry was occuring. The C_3H_7OOH PIE curve was similar in shape to the PIE taken with the OxCl chemistry, but had a slightly earlier appearance energy. Poor mass resolution for the PIE was a problem at some m/z as shown for C_3H_7, but the shape of C_3H_7 was similar to that from the OxCl chemistry.

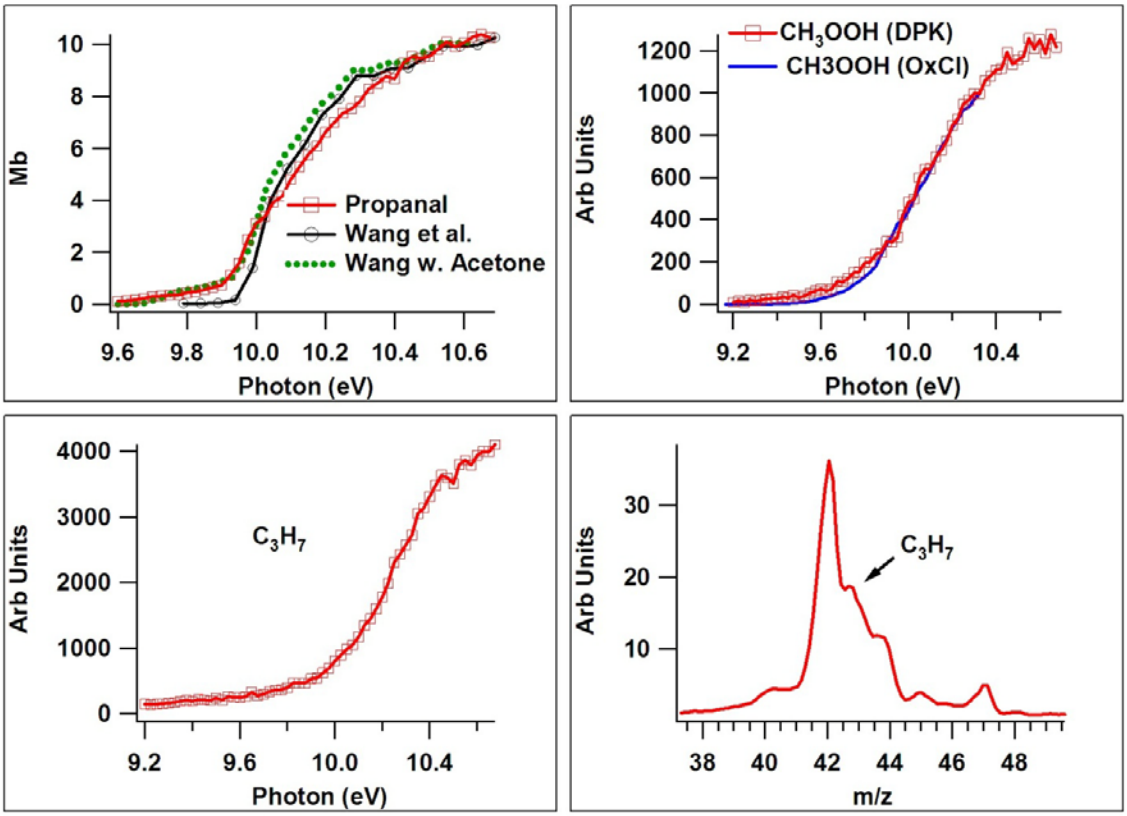

Figure 3-24. PIE identification using the DPK precursor chemistry for $C_3H_7O_2$

Larger molecular weight products were not observable because of the need to avoid signal saturation due to the DPK precursor similar to the acetone and DEK chemistry.

3.3.3.2.b Measurement of α

Without a confident determination of the major products it was not possible to measure α. Assuming that C_2H_5CHO was detected at m/z 58 and that no C_3H_7OH was detected, would imply an $\alpha = 1$. Further experiments are needed before this can be reliably stated given the unknown masses observed.

3.4 Discussion

3.4.1 $C_2H_5O_2$ self reaction

In this work α for the $C_2H_5O_2$ self reaction was measured during Run 1A and Run 2. The measured value for each run was different. Run 2 was the stronger set of data and was the basis of the overall results. Run 1A had complications resulting from secondary chemistry of the products on the walls of the flow tube. The value of α measured during Run 1A was in agreement with end product studies in the literature so the secondary chemistry that was observed in Run 1A may explain some of the other literature results as well.

3.4.1.1 Run 1A compared with Run 2: Observed Products

The first clear difference between Run 1A and 2 was the pump out portion of the individual mass time traces. By comparing **Figure 3-2** and **Figure 3-11** it is clear that the incomplete pump out of C_2H_5OH and C_2H_5OOH in Run 1A was not a problem in Run 2. In this system wall interactions were unavoidable, and sometimes a clean tube required a certain amount of use before the walls became passivated. Prior to Run 1A a clean tube was inserted, which may have not had enough preliminary runs to passivate it. This could have led to preferential sticking of the hydroxyl and hydroperoxyl species. In one kinetics model fit a wall equilibrium was introduced for C_2H_5OH and α was fixed at 0.30 based on the data from Run 2. K_{eq} values ranged from 0.9 – 1.1 with forward and reverse rates ranging over 300 – 400 s^{-1}. The rate constants needed appear to be a little fast to reasonably explain the data. However the JPL work has found diffusion rates for $C_2H_5O_2$ of 5 – 10 s^{-1} at 50 Torr.[28] Directly proportional diffusion rates would be 68 – 125 s^{-1} at 4 Torr. Given the uncertainty in the absolute rate constants from the data already discussed it is possible that wall loss could have played a role in the α measured.

Wall chemistry also may have played a role in the other noticeable difference between Run 1A and Run 2, the extra mass peaks. Comparing the 1-D mass spectrums in **Figure 3-4** and **Figure 3-12** the data from Run 1A had much larger relative mass peaks at m/z 45 and 47 than in Run 2. **Table 3-1** shows all the additional peaks discussed during the results section of Run 1A that did not appear in Run 2. The peroxy hemiacetal chemistry assigned in Run 1A is supported by the fact that when no m/z 106 peak was seen in Run 2 the m/z 45 dissociation product was also greatly reduced. Some small amount of secondary chemistry was still occurring in Run 2, as evidenced by the occasional detection at m/z 90, but it appeared to play a much smaller role in the overall chemistry. Although much smaller, the peak at m/z 45 in Run 2 was still larger than would be expected from isotopic abundance alone. One other possible source was a small amount of dissociative ionization from C_2H_5OH. Dissociative ionization is not reported to occur until 10.8 eV,[15] but reaction (3.1) is exothermic by 350 kJ/mol so it is possible that some excited C_2H_5OH was cracking during ionization at lower than expected energies. A last possibility was dissociative ionization of C_2H_5OOH, but experimental and theoretical work by Li et al. shows that the first electron removed is a non-bonding electron on the O atom leading to a tighter O-O bond, not dissociation.[21]

The m/z 47 peak was unexplained in both Run 1A and Run 2. As with m/z 45 it was partially due to an isotopic peak of ethanol, but was also larger than expected. The time trace appears almost as a step function indicating a stable product from the formation chemistry. The time trace taken together with the odd mass number means that it was likely to have come from a dissociative ionization process, because a radical would have undergone further reaction.

At higher mass, one complication with a secondary chemistry explanation of the m/z 106 time trace was the speed with which the product grew in. **Figure 3-5** shows the time dependence of m/z 106 to be as fast as that of the primary products. If secondary surface chemistry was responsible a slower appearance would have been expected similar to what was observed at m/z 90. One explanation is that some wall absorption of the ethanol and ethyl hydroperoxide remains between shots helping to jump start the chemistry after the next pulse.

The formation chemistry of the $C_2H_5O_2$ was not affected by the use of 193 nm or 248 nm excimer light for the photolysis of OxCl. No difference was seen between the mass spectrum of the 4 Torr 193 nm and 248 nm photolysis data sets in Run 2. This suggests that reactions of the $ClCO^*$ fragment before it falls apart were not important in the 248 nm photolysis, and that the unexplained mass peaks did not involve $ClCO^*$ chemistry.

Overall the larger mass interferences in Run 1A can be explained by further reactions of the products from the $C_2H_5O_2$ self reaction. This additional chemistry combined with the observed wall interactions skewed the measured amounts of the stable products.

3.4.1.2 Run 1A compared to Run 2: Measurement of α and other R

In both runs the absolute kinetics determined rate constants which could be as much as 2 – 4 times that of the literature values. This results from the difficult nature of determining the absolute calibration factors for the experiment. As discussed in the Results and Analysis section, in Run 1A the monochromator slits were accidentally adjusted during the calibration run leading to uncertainty in the total photon count. The

general quality of the fits in Run 1A was good, as can be seen in **Figure 3-2**, whereas the quality of the fit was not as good for all the time traces simultaneously in Run 2. **Figure 3-11** shows a number of the fits, each of which were able to represent some of the time traces. The C_2H_5OH and C_2H_5OOH time traces appeared more in sync, but the CH_3CHO had a rapid rise not seen in the other masses. An early source of CH_3CHO is not known. Reactions (3.22) and (3.23) have been looked for but are negligible for room temperature experiments.[25,29]

$$C_2H_5 + O_2 \longrightarrow c - C_2H_4O + OH \tag{3.22}$$

$$C_2H_5 + O_2 \longrightarrow CH_3CHO + OH \tag{3.23}$$

The imperfect time trace agreement between all the stable products in Run 2 was the only outstanding issue with those data sets. For both runs the relative nature of the α measurement meant that it was not affected by the uncertainty in the calibration factor and the values from the kinetics fits were in good agreement with the values obtained from *R*. This agreement helped validate the steady state approximation used in the derivation of *R*.

The other ratios $R_{A/EH}$ and $R_{E/EH}$ showed different behavior in Run 1A and Run 2, potentially shedding further light on why the two runs differ. The most striking feature of a comparison between **Figure 3-8** and **Figure 3-15** is the behavior of $R_{E/EH}$ for Run 1A during the pump out. This displays again the different nature of the pump out process for the different stable products. In Run 2 C_2H_5OOH was pumping out more slowly than the other products, but it was not as large a difference as seen in Run 1A.

The value of α measured in Run 2 was the best determination. Problems with additional chemistry probably threw off the value of α in Run 1A. Absolute kinetics were

not reliable from either run, so more attention needs to be paid to the calibration runs in the future to determine absolute rate constants.

3.4.1.3 Photoionization cross section of C_2H_5OOH

The photoionization cross section of C_2H_5OOH was measured relative to the values of CH_3CHO, C_2H_5OH, and C_2H_4. Each of these species has known cross sections given in the experimental section. All production of C_2H_5OOH can be quantitatively linked to the concentrations of these three species if you assume that C_2H_5OOH was only produced by reaction (3.5). This means finding all the sources of HO_2 which was produced initially in equal amounts with C_2H_4, and also by reaction of C_2H_5O with O_2. Therefore C_2H_4 determines the initial amount, and the comparison of CH_3CHO with C_2H_5OH determines the amount produced from C_2H_5O, so all sources are covered. One downside is that this value is not entirely independent of the kinetics, which would have been desirable given their inaccuracy, because it does depend on the overall rate of production C_2H_5OOH from the kinetics model. The reported value of 2.57 Mb at 10.7 eV was determined from Run 2 data sets where the chemistry was better understood. The error in this measurement was difficult to determine, but given the uncertainty in the kinetics fits a reasonable estimate is that it is good to within a factor of 2.

3.4.2 CH_3O_2 self reaction

Overall the CH_3O_2 data was very promising, but there were not enough data sets to make a definitive measurement of α. The mass resolution and species assignments were mostly straightforward. An alternative chemistry for producing CH_3O_2 would be useful to allow investigation of larger product masses, but there were no significant product masses at lower weight which appeared as though they might come from a larger

parent. The only complication in the data was the transient peak at m/z 32 on top of the CH_3OH signal. If this is persistent, coming perhaps from excited O_2, then it will cause some problems with the data, but it appears that it does not last long in time so it is safe to treat the data later on as free from contamination. More data is necessary to answer these questions, but the approach appears very promising.

3.4.3 $C_3H_7O_2$ self reaction

Neither the OxCl or DPK chemistry provided a clear story of the $C_3H_7O_2$ self reaction. As was expected the non-isomer-specific OxCl chemistry led to challenges with identification of the products. What was not expected was that the 1-$C_3H_7O_2$ isomer-specific DPK chemistry products also did not exactly match the expected PIE curves. In each case it was not exactly clear why the PIE curves could not be matched well. In principle a quantitative fit to the PIE curves at one mass using reference PIEs for the two isomers could determine the contribution of each isomer and allow for determination of α. This assumes they have a nearly identical time dependence, i.e., that the two RO_2 isomers have similar self reaction rate constants. Therefore this data did not make it possible to determine whether a better data set or better chemistry approach is needed. There did appear to be specific difficulties that were common to each initiation chemistry regardless of RO_2, but these will be discussed further below. Overall an approach that separates the isomers by initiation chemistry is more appealing, but it should not be required if other factors are more of a problem.

3.4.4 Ketone initiation chemistry

Acetone, DEK, and DPK were all used as photolytic precursors for their corresponding RO_2 radicals through reactions (3.14), (3.13), and (3.17). The major

downside of this production method was the inability to look for the ROOR or other high molecular weight products due to the necessity of avoiding signal saturation from the parent ketone by moving large masses off the detector. This problem aside, the ketone chemistry was expected to be a clean source of alkyl radicals for production of RO_2 by reaction (3.6). The acetone chemistry appeared to work this way, and only an insufficient number of data sets taken prevented a definitive measurement of α from being made. The DEK and DPK chemistries were not as straightforward . This was disappointing especially for the DPK case where the corresponding OxCl chemistry led to multiple isomers. For both DEK and DPK strong signals were obsesrved at the expected aldehyde mass (m/z 44 or m/z 58), but not much product was observed for the corrseponding alcohol product (m/z 46 or m/z 60) as can be seen by comparing **Figure 3-10** and **Figure 3-23**. Another similarity can be seen by looking at the time trace of C_2H_5 and C_3H_7 in **Figure 3-9** and **Figure 3-23**. In both cases there was a fast initial drop in radical followed by a slower reaction trace more indicative of the RO_2 self reaction chemistry. It is possible that some of the initial HO_2 created reacts with still unreacted R.

$$R + HO_2 \longrightarrow R'CHO + H_2O \qquad (3.24)$$

This type of reaction has mainly been investigated for R = CH_3 and has been looked at predominantly at higher temperatures for combustion chemistry purposes.[30,31] There has been one experimental study for R = C_2H_5, but it found a relatively slow bimolecular rate constant of $k_{1.24}$ = 3.1 x 10^{-13} cm^3 $molecules^{-1}$ s^{-1} at room temperature.[32] Large O_2 concentrations mean that reactions (3.6) and (3.7) will be much faster, especially as the size of R increases.[33] These difficult to explain time traces, combined with the skewed

product distribution, suggests that except for acetone, the ketone chemistry may not be a good source of alkyl radicals for product analysis of the RO_2 self reaction.

3.4.5 Oxalyl chloride initiation chemistry

There were also similarities among the OxCl chemistry data sets across RO_2. The high radical concentration OxCl chemistry for $C_2H_5O_2$ and $C_3H_7O_2$ both had problems with pump out of the alcohol and hydroperoxide (**Figure 3-2** and **Figure 3-20**). It is not clear if the problem was common to both chemistries because they were done right after each other in time, or whether it was related to the high radical concentrations present. These runs also had evidence of high molecular weight products that appeared to be from wall reactions. In Run 2 of the $C_2H_5O_2$ self reaction the OxCl concentration was reduced an order of magnitude and the reaction chemistry occurred cleanly without any pump out or high molecular weight product issues. Radical concentration was probably an important factor, but so was the overall chemistry because the ketone chemistry just discussed was also of lower radical concentration, but was not as reliable.

3.4.6 Comparison with literature

3.4.6.1 $C_2H_5O_2$

The majority of previous studies on α of the $C_2H_5O_2$ self reaction have been done by end product analysis on the time scale of minutes after the reaction. Chapter 2 described the only previous study to determine α on the time scale of the reaction by detecting the secondary HO_2 produced from the reaction sequence of (3.2) and (3.4). The value of α determined by this method was half the value determined previously by the end product studies. This experiment was able to perform a similar end product analysis

as the initial studies, but on the same time scale as the reaction to prevent any unknown secondary chemistry from distorting the observed ratios.

There have been six previous studies that measured α for the $C_2H_5O_2$ self reaction. Two of these, the Kaiser et al.[34] work and the Anastasi et al.[35] were superseded by new work from the same group and never published in the peer reviewed literature, and will not be discussed further. The other studies are all plotted in **Figure 3-25**.[28,36-38]

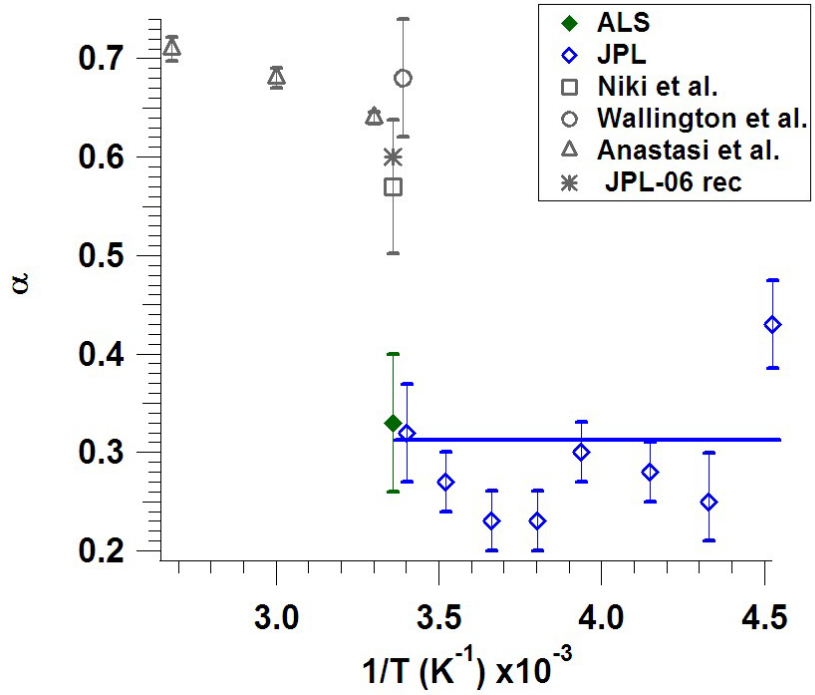

Figure 3-25. Comparison of α measurements. JPL and ALS work both made measurements on the time scale of the reaction.

Chapter 2 summarized the differences between that work and the others.This work provided a bridge between all of the previous work because it was done on the same time scale of the reaction similar to Chapter 2, but detected all of the stable products similar to the end product studies. The Run 1A data measured an α that was in agreement with the older end product studies, but the data plotted in **Figure 3-25** is from Run 2 and is in best agreement with the Chapter 2 measurement (Labeled as "JPL"). Run 2 was

settled on as the better data set because of secondary chemistry complications in Run 1A. If the comparison of Run 1A and Run 2 serves as a model for what might lead to the difference between the Run 2 result and the other end product studies, then additional secondary chemistry could be the reason for the higher values of α measured by the end product studies. As an example, the flash photolysis experiment from the Chapter 2 work was immune to surface chemistry so it would not have been affected by hemi-acetal reactions (3.18) and (3.19), but The FTIR studies of Niki et al. and Wallington et al. would have been prone to these interfering reactions.[37,38] The different values from Run 1A and Run 2 show that under certain conditions this work was also susceptible to wall chemistry, but suitable conditions could be achieved where the interference was negligible.

One further type of wall chemistry not previously considered is the conversion of hydroperoxides to aldehydes through the dehydration shown in reaction (3.25). Evidence for this has been found both in the original synthetic studies on hydroperoxides and in more recent work investigating the raman spectroscopy of the hydroperoxides.[39,40]

$$C_2H_5OOH \longrightarrow CH_3CHO + H_2O \qquad (3.25)$$

Production of water would have been a signature of this occuring, but the IP of water was above the energy at which we took data so it could not be identified. Still, the simplest and most plausible explanation for the differences observed are that higher radical concentrations of the literature and Run 1A work allowed for wall chemistry that interfered with the main products.

3.4.6.2 CH_3O_2

A full comparison with the literature for the CH_3O_2 self reaction is premature given the single measurement made with this work. Still that measurement ($\alpha = 0.53$) is outside the range of previous measurements and the recommended value, $\alpha = 0.28 – 0.43$, 0.37 recommended.[1] The $C_2H_5O_2$ value was also outside the range of previous measurements, but it was lower rather than higher. If this value were to hold up it might indicate a completely different trend with alkyl group than anticipated. As discussed last chapter, the uncertainty in the mechanism of the RO_2 self reaction raised by recent theoretical work makes it difficult to predict what the trend with R group should be.[41] Further experimental work looking at the nascent products may be able to guide the theory as to what pathways are important.

3.4.6.3 $C_3H_7O_2$

No measurement of α was possible with the preliminary data recorded here, but there are only two previous determinations for the self reaction of 2-$C_3H_7O_2$.[2,3] Both these studies are end product studies using GC or GC/MS, so further work would be very useful. If a new trend in α with RO_2 was expected, confirmation from work on a larger RO_2 such as $C_3H_7O_2$ would be essential.

3.5 Conclusion

In this work the RO_2 self reactions for R = CH_3, C_2H_5, and C_3H_7 have been investigated using a time resolved photoionization mass spectrometer to allow for real time detection of the reaction products. Products and reactants of the reactions were identified by both their time traces and their PIE curves. The radical product channel branching fraction, α, was measured to be 0.33 ± 0.08 for the $C_2H_5O_2$ self reaction. This

value was in agreement with the work in Chapter 2 that also made measurements of α on the timescale of the reaction, but disagrees with previous end product studies. Preliminary data for the CH_3O_2 and $C_3H_7O_2$ self reactions were also obtained. More data is needed to make a definitive determination of α for these reactions, but a good understanding of complications from different precursor chemistries should make further measurements simpler.

3.6 References

(1) Tyndall, G. S.; Cox, R. A.; Granier, C.; Lesclaux, R.; Moortgat, G. K.; Pilling, M. J.; Ravishankara, A. R.; Wallington, T. J. *Journal of Geophysical Research-Atmospheres* **2001**, *106*, 12157.

(2) Cowley, L. T.; Waddington, D. J.; Woolley, A. *Journal of the Chemical Society-Faraday Transactions I* **1982**, *78*, 2535.

(3) Kirsch, L. J.; Parkes, D. A.; Waddington, D. J.; Woolley, A. *Journal of the Chemical Society-Faraday Transactions I* **1979**, *75*, 2678.

(4) Lightfoot, P. D.; Lesclaux, R.; Veyret, B. *Journal of Physical Chemistry* **1990**, *94*, 700.

(5) Osborn, D. L.; Zou, P.; Johnsen, H.; Hayden, C. C.; Taatjes, C. A.; Knyazev, V. D.; North, S. W.; Peterka, D. S.; Ahmed, M.; Leone, S. R. *Review of Scientific Instruments* **2008**, *79*.

(6) Wu, C. Y.; Lee, Y. P.; Ogilvie, J. F.; Wang, N. S. *Journal of Physical Chemistry A* **2003**, *107*, 2389.

(7) Hall, G. E.; Metzler, H. W.; Muckerman, J. T.; Preses, J. M.; Weston, R. E. *Journal of Chemical Physics* **1995**, *102*, 6660.

(8) Reid, J. P.; Marcy, T. P.; Kuehn, S.; Leone, S. R. *Journal of Chemical Physics* **2000**, *113*, 4572.

(9) Weir, D. S. *Journal of the American Chemical Society* **1961**, *83*, 2629.

(10) NIST Chemistry WebBook, http://webbook.nist.gov/chemistry/, 2009.

(11) Baklanov, A. V.; Krasnoperov, L. N. *Journal of Physical Chemistry A* **2001**, *105*, 97.

(12) Lightfoot, P. D.; Kirwan, S. P.; Pilling, M. J. *Journal of Physical Chemistry* **1988**, *92*, 4938.

(13) Choi, N.; Pilling, M. J.; Seakins, P. W.; Wang, L. *Physical Chemistry Chemical Physics* **2006**, *8*, 2172.

(14) Knyazev, V. D.; Slagle, I. R. *Journal of Physical Chemistry A* **2001**, *105*, 6490.

(15) Cool, T. A.; Wang, J.; Nakajima, K.; Taatjes, C. A.; McIlroy, A. *International Journal of Mass Spectrometry* **2005**, *247*, 18.

(16) Cooper, G.; Anderson, J. E.; Brion, C. E. *Chemical Physics* **1996**, *209*, 61.

(17) Cool, T. A.; Nakajima, K.; Mostefaoui, T. A.; Qi, F.; McIlroy, A.; Westmoreland, P. R.; Law, M. E.; Poisson, L.; Peterka, D. S.; Ahmed, M. *Journal of Chemical Physics* **2003**, *119*, 8356.

(18) Wang, J.; Yang, B.; Cool, T. A.; Hansen, N.; Kasper, T. *International Journal of Mass Spectrometry* **2008**, *269*, 210.

(19) Hsu, W. L.; Tung, D. M. *Review of Scientific Instruments* **1992**, *63*, 4138.

(20) FACSIMILE; 4.0.36 ed.; MCPA Software Ltd. 2002.

(21) Li, Y. M.; Sun, Q.; Li, H. Y.; Ge, M. F.; Wang, D. X. *Chinese Journal of Chemistry* **2005**, *23*, 993.

(22) Tobias, H. J.; Docherty, K. S.; Beving, D. E.; Ziemann, P. J. *Environmental Science & Technology* **2000**, *34*, 2116.

(23) Leach, S.; Schwell, M.; Jochims, H. W.; Baumgartel, H. *Chemical Physics* **2006**, *321*, 171.

(24) Wood, K. V.; Taylor, J. W. *International Journal of Mass Spectrometry and Ion Processes* **1979**, *30*, 307.

(25) Clifford, E. P.; Farrell, J. T.; DeSain, J. D.; Taatjes, C. A. *Journal of Physical Chemistry A* **2000**, *104*, 11549.

(26) Wagner, A. F.; Slagle, I. R.; Sarzynski, D.; Gutman, D. *Journal of Physical Chemistry* **1990**, *94*, 1853.

(27) Meloni, G.; Zou, P.; Klippenstein, S. J.; Ahmed, M.; Leone, S. R.; Taatjes, C. A.; Osborn, D. L. *Journal of the American Chemical Society* **2006**, *128*, 13559.

(28) Noell, A. C. A., L.N.; Robichaud, D. J.; Okumura, M.; Sander, S.P. **Manuscript in preparation**.

(29) DeSain, J. D.; Klippenstein, S. J.; Miller, J. A.; Taatjes, C. A. *Journal of Physical Chemistry A* **2003**, *107*, 4415.

(30) Jasper, A. W.; Klippenstein, S. J.; Harding, L. B. *Proceedings of the Combustion Institute* **2009**, *32*, 279.

(31) Zhu, R. S.; Lin, M. C. *Journal of Physical Chemistry A* **2001**, *105*, 6243.

(32) Ludwig, W.; Brandt, B.; Friedrichs, G.; Temps, F. *Journal of Physical Chemistry A* **2006**, *110*, 3330.

(33) Ruiz, R. P.; Bayes, K. D. *Journal of Physical Chemistry* **1984**, *88*, 2592.

(34) Kaiser, E. W.; Rimai, L.; Wallington, T. J. *Journal of Physical Chemistry* **1989**, *93*, 4094.

(35) Anastasi, C. B., M.J.; Smith, D.B.; and Waddington, D.J. Joint Meeting of the French and Italian Sections of the Combustion Institute, June 1987, Amalfi.

(36) Anastasi, C.; Waddington, D. J.; Woolley, A. *Journal of the Chemical Society-Faraday Transactions I* **1983**, *79*, 505.

(37) Niki, H.; Maker, P. D.; Savage, C. M.; Breitenbach, L. P. *Journal of Physical Chemistry* **1982**, *86*, 3825.

(38) Wallington, T. J.; Gierczak, C. A.; Ball, J. C.; Japar, S. M. *International Journal of Chemical Kinetics* **1989**, *21*, 1077.

(39) Jacob, P.; Wehling, B.; Hill, W.; Klockow, D. *Applied Spectroscopy* **1997**, *51*, 74.

(40) Rieche, A.; Hitz, F. *Berichte Der Deutschen Chemischen Gesellschaft* **1929**, *62*, 2458.

(41) Ghigo, G.; Maranzana, A.; Tonachini, G. *Journal of Chemical Physics* **2003**, *118*, 10575.